

國立交通大學

光電工程研究所
碩士論文

不同電極對下電極結構之非晶系銦鎵鋅氧化
薄膜電晶體之影響

Effects of Source and Drain Electrode Types on
Bottom Contact Amorphous-Indium-Gallium-Zinc-Oxide
Thin-Film Transistors

研究 生：吳高銘

指 導 教 授：謝漢萍 教 授

中華民國九十八年六月

不同電極對下電極結構之非晶系銦鎵鋅氧化 薄膜電晶體之影響

Effects of Source and Drain Electrode Types on Bottom Contact Amorphous Indium-Gallium-Zinc-Oxide Thin-Film Transistors

研究 生：吳高銘

Student : Gao-Ming Wu

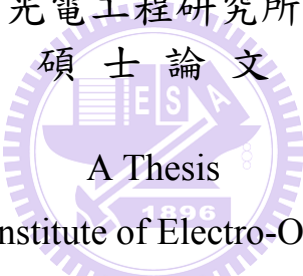
指 導 教 授：謝漢萍

Advisor : Han-Ping D. Shieh

國立交通大學 電機學院

光電工程研究所

碩士論文



A Thesis

Submitted to the Institute of Electro-Optical Engineering

College of Electrical and Computer Engineering

National Chiao Tung University

in partial Fulfillment of the Requirements

for the Degree of Master

in

Electrical-Optical Engineering

June 2009

Hsinchu, Taiwan, Republic of China

中華民國九十八年六月

不同電極對非晶系銻鎵鋅氧薄膜電晶體之影響

學生：吳高銘

指導教授：謝漢萍

國立交通大學光電工程研究所

摘要

藉由探討氧通量，退火，半導體與介電層介面性質，與不同電極材料的變化，研究了不同製程因素對於銻鎵鋅氧薄膜的特性影響，以提升非晶系銻鎵鋅氧薄膜電晶體的效能。一開始，先藉由氧通量的變化，來探討氧通量對薄膜特性的影響，而優化薄膜的半導體特性。另一方面，藉由退火改善了半導體與介電層的介面特性，結果隨著退火時間增長，臨界電壓會減小。進一步的，藉由引入介面修飾層，來探討半導體與介電層介面特性，找出適合銻鎵鋅氧的接觸面性質，而發現疏水性的 HMDS 改善了載子遷移率。接下來，藉由探討不同電極材料之功函數與接觸阻抗的關係，對下電極結構之非晶系銻鎵鋅氧薄膜電晶體效能的影響，進而找出適合匹配銻鎵鋅氧的電極材料，用來改善非晶系銻鎵鋅氧薄膜電晶體的效能，結果鈦電極展現了最佳的特性。最後，因為不具通道保護層的裝置會與環境中的水氧反應，而進一步討論了臨界電壓隨時間減小的不穩定性。

Effects of Source and Drain Electrodes on

Amorphous Indium-Gallium-Zinc-Oxide

Thin-Film Transistors

Student : Gao-Ming Wu

Advisor : Dr. Han-Ping D. Shieh

**Institute of Electro-Optical Engineering
National Chiao Tung University**



Via investigating the oxygen and annealing effects, interface property, and source/drain materials, high performance a-IGZO TFT was fabricated. First, the oxygen flow rate was varied to examine oxygen absorption effect. Post-annealing improves the bonding in a-IGZO because of the semiconductor/insulator interface modification. The device mobility can be up to $11.42 \text{ cm}^2(\text{Vs})^{-1}$. Second, the dual stack a-IGZO TFT structure is introduced to examine the properties of the a-IGZO/gate insulator interface. HMDS-buffered a-IGZO TFT has larger mobility, implying improved channel/dielectric interfacial condition when it is stacked with the hydrophobic material HMDS. Following, the effects of source/drain electrode types on a-IGZO TFT were investigated. The performance of the a-IGZO TFT with Ti source/drain electrodes is appropriate for the display applications. Finally, the ambient effect was discussed. The water molecule absorption dominates the a-IGZO ambient interaction in ambience and the threshold voltage shifts negatively.

誌 謝

首先要感謝指導教授謝漢萍院長為我們建立了一個資源豐富的研究環境，兩年的碩班生涯著實令我受益良多。除了設備完善讓我們可以有世界級的研究成果，高水準的師資與研究團隊可以隨時與世界頂尖研究成果爭雄，實驗室注重英文能力等精神也讓我們不忘踏出關門研究的階段，培養國際化的視野，成為更全方位的人才，可以在未來為校爭光，回饋培育我們的社會。另一方面也感謝黃乙白教授與鄭惟中教授的照顧，與華映及交映樓學長同學們的幫忙。

在實驗的過程中我最感謝我的好夥伴朱益興。他與我在無塵室內，量測機台邊共度無數時光。有漫漫長夜，有破曉時分，擁有得來不易的令人欣慰的成果時，喜悅可以共享。也感謝學長莊喬舜也不時給關心我們並給予指點並有情有義的帶著我們畢業。

最後最重要的，我要感謝的父母家人，他們的養育之恩，栽培之情，與不離不棄的陪伴，比任何言語都要深刻而有力的支持著我，我會用一切的努力來報答。

Table of Contents

Abstract (Chinese).....	i
Abstract (English).....	ii
Acknowledgements.....	iii
Table of Content.....	iv
Figure Caption.....	v
List of Tables.....	vi
Chapter 1 Introduction.....	13
 1.1. Amorphous	
Semiconductors.....	13
 1.2. Amorphous Oxide Semiconductors.....	15
 1.2.1. The Introduction to Amorphous Oxide Semiconductors.....	15
 1.2.2. The Carrier Transport Mechanism of AOSs.....	16
 1.3. Amorphous In-Ga-Zn-O Thin Film Transistors.....	17
 1.3.1. Introduction.....	17
 1.3.2. The $\text{In}_2\text{O}_3\text{-}\text{Ga}_2\text{O}_3\text{-}\text{ZnO}$ Ternary System.....	18
 1.3.3. The a-IGZO TFT State of the Art.....	22
 1.4. Motivation	25
 1.5. Thesis Organization	26
Chapter 2 Principles and Characterization.....	27
 2.1. Thin Film Transistor and Operation.....	27
 2.2. Electrical Measurement.....	30
 2.3. Parameter Extraction Method.....	30

2.3.1. Determination of the Threshold Voltage.....	30
2.3.2. Determination of the Subthreshold Swing.....	31
2.3.3. Determination of the Field-Effect Mobility.....	32
2.3.4. Determination of the On/Off Current Ratio.....	33
2.4. Surface Morphology Measurement.....	33
2.5. Contact Angle Measurement.....	35

Chapter 3 Experimental Methods.....37

3-1. a-IGZO TFT Device Fabrication.....	37
3-2. Sputtering.....	30
3.2.1. RF sputtering.....	41
3.2.2. DC sputtering.....	42



Chapter 4 Experimental Results and Discussion.....44

4-1. The Effects of Oxygen Flow Rate and Post-Annealing on a-IGZO TFTs.....	44
4.1.1. Introduction.....	44
4.1.2. Results and Discussion.....	47
4.1.2.1. Determination of the Deposition Rate.....	47
4.1.2.2. The Effects of Oxygen Flow Rate on a-IGZO TFTs.....	48
4.1.2.3. The Effects of Post-Annealing on a-IGZO TFTs	51
4.1.3. Conclusion.....	52
4-2. The Interface Modification for a-IGZO TFTs.....	53
4.2.1. Introduction.....	53
4.2.2. Result and Discussion	54
4.2.3. Conclusion	57
4-3. The Effects of Source and Drain Electrodes on a-IGZO TFTs.....	58
4.3.1. Introduction	58
4.3.2. Result and Discussion	60

4.3.2.1. The Effects of Source/Drain electrodes on a-IGZO TFTs	60
4.3.2.2. The Ambience Effect on a-IGZO TFTs.....	64
4.3.3. Conclusion	68
Chapter 5 Conclusion.....	70
5-1. Conclusion.....	70
5-2. Future Work.....	72
References.....	74

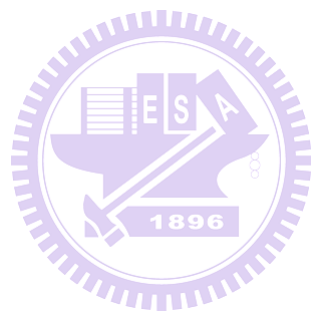


Figure Caption

Fig. 1-1 History of amorphous semiconductors on new fields.....	2
Fig. 1-2 Flexible transparent TFTs (TIFTs) (a) A photograph of the flexible TFT sheet bent at $R = 30$ mm. The TFT sheet is fully transparent in the visible light range (b) A photograph of the flexible TFT sheet. The transparent TFT devices are made visible by adjusting the angle of the illumination ²	3
Fig. 1-3 Schematic orbital drawing of electron pathway (conduction band bottom) in conventional silicon-base semiconductor and ionic oxide semiconductor. ²	5
Fig. 1-4 Transmittance of a-IGZO film in visible light region.....	7
Fig. 1-5 The amorphous formation region (right) and the electron mobilities and concentrations evaluated from the Hall effects for the amorphous thin films (left) in the In_2O_3 - Ga_2O_3 - ZnO system. The thin films were deposited on a glass substrate by PLD under deposition atmosphere of $P_{\text{O}_2} = 1$ Pa. Number in the parenthesis denotes carrier electron concentration. ¹	8
Fig. 1-6 The carrier concentration as a function of O_2 pressure during the deposition in a- InGaZnO_4 and a- $\text{In}_2\text{Zn}_3\text{O}_6$. ¹	9
Fig. 1-7 (a) The display image of LG's 3.5" AMOLED (b) Samsung's AMOLED display driven by InGaZnO TFT.....	11
Fig. 1-8 The display image of Samsung's 12.1" WXGA AMOLED display ^{6,7} ..	13
Fig. 2-1 A bottom-gate-top-contact TFT structure.....	17
Fig. 2-2 The semiconductor energy band diagram when (a) unbiased, (b) negative gate voltage bias, (c) positive gate voltage bias.....	18
Fig. 2-3 A schematic model of atomic force microscope.....	23
Fig. 2-4 The contact angle formation of liquid on solid surface.....	24
Fig. 3-1 The flow chart of typical a-IGZO TFT device fabrication.....	28

Fig. 3-2 Schematic RF sputtering system.....	31
Fig. 3-3 Schematic DC sputtering system.....	32
Fig. 4-1 The carrier source of (a) Si, (b) Metal oxide.....	34
Fig. 4-2 Electrical property of IGZO TFT as a function of oxygen and argon flow rate during deposition. ⁶	35
Fig. 4-3 The AFM result of (a) 0 sccm O ₂ device deposited for 6.5 mins. (b) 0.6 sccm O ₂ device deposited for 8 mins.....	36
Fig. 4-4 The a-IGZO TFT output characteristics for different oxygen flow rates.....	38
Fig. 4-5 Annealing 0 to 2 hours for devices of O ₂ flow rate: (a) 0 sccm, (b) 0.6 sccm.....	39
Fig. 4-6 The output electrical characteristic comparison for a-IGZO TFTs post-annealed for 2 and 3 hours.....	41
Fig. 4-7 The dual stack a-IGZO TFT structure.....	43
Fig. 4-8 I _D -V _G curve comparison of the buffered-a-IGZO TFTs.....	44
Fig 4-9 Contact angle image for water drop on the (a) Al ₂ O ₃ , (b) HfO ₂ , (c) HMDS, and (d) SiO ₂ surface.....	45
Fig. 4-10 The electrical characteristics comparison for a-IGZO TFTs with different source/drain electrodes.....	49
Fig. 4-11 The work functions of some metallic materials.....	50
Fig. 4-12 The contact resistance comparison for different source/drain electrodes.....	51
Fig. 4-13 The schematic diagram showing the role of (a) oxygen as an electron acceptor and (b) water molecules as a electron donor onto a-IGZO surface. ¹⁴	54
Fig. 4-14 The negative shift of the threshold voltage over time for a-IGZO TFT with (a) Ti, (b) ITO, (c) Au, and (d) Al source/drain electrodes.....	56
Fig. 5-1 The Canon's proposed devise structure on SID' 08.....	62
Fig. 5-2 The a-IGZO layer with the Si ₃ N ₄ passivation layer.....	62

Fig. 5-3 The proposed structure for a-IGZO passivation.....63



List of Tables

Table 3-1 The electrode fabrication methods.....	29
Table 4-1 Contact angle of different buffer layer surface.....	45
Table 4-2 The performance of the a-IGZO TFTs with the interface modification layer.....	46
Table 4-3 Electrical properties comparison for varied electrodes.....	53

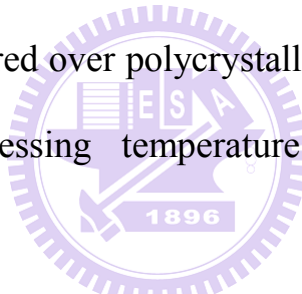


Chapter 1

Introduction

1.1. Amorphous Semiconductors

An important semiconductor feature is the carrier concentration controllability over several orders of magnitude. Amorphous semiconductors are preferred over polycrystalline ones for active layers from the viewpoints of processing temperature and uniformity of device characteristics.



Research on amorphous semiconductors started in 1950s to seek appropriate materials. Fig. 1-1 summarizes the brief history of amorphous semiconductors. The largest impact on electronics is the discovery of hydrogenated amorphous silicon (a-Si:H) by Spear and LeComber in 1975. This is the first material which can control carrier concentration by impurity doping as in crystalline, and it opened a new frontier called ‘Giant Microelectronics’ which means electronics based on circuits fabricated on a large area substrate. Nowadays, active-matrix flat-panel display (AMFPD) circuits mainly use a-Si:H thin film transistors (TFTs).

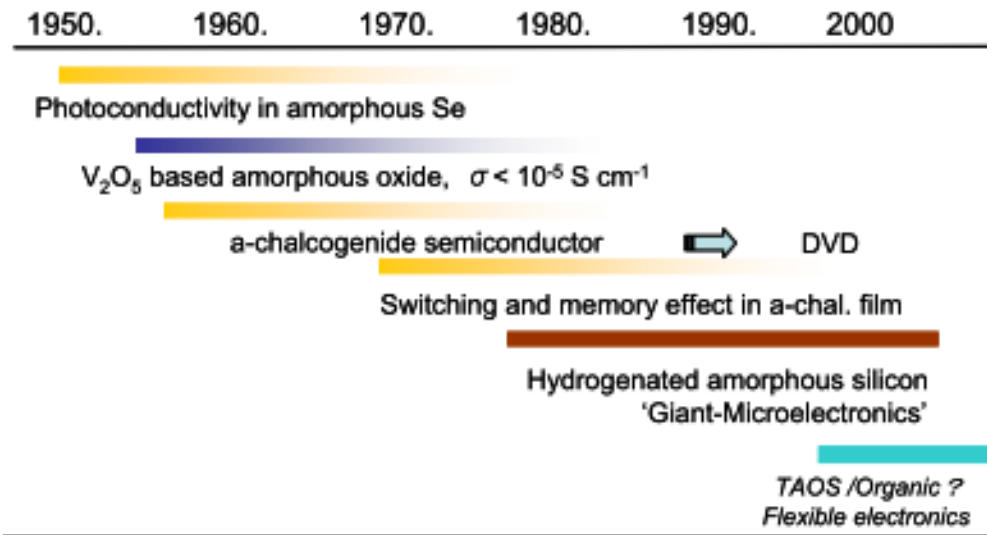


Fig. 1-1 History of amorphous semiconductors on new fields.¹

Recently, a new electronics is emerging for applications which cannot be fabricated by Si MOS technology. This frontier “flexible electronics” is characterized by electronic circuits fabricated on organic (flexible substrates) instead of inorganic (hard) glasses. The flexible electronic area was born to meet a strong demand for large-area displays because glass substrates are heavy and fragile, and are obviously inconvenient. Amorphous semiconductors are much preferable than crystalline semiconductors for flexible electronics. So far, organic molecule semiconductors have been almost exclusively examined for such applications but their performance and chemical instability are not sufficient for practical applications. Further, the field-effect mobilities of organic TFTs are too low to drive high-resolution,

high speed active matrix organic light emitting diode (AMOLED) displays.¹

1.2. Amorphous Oxide Semiconductors

1.2.1. Introduction to Amorphous Oxide Semiconductors

Amorphous oxide semiconductors (AOS) are materials for high performance, low processing temperature electronic devices such as flexible devices due to their high electron mobility $\gg 10 \text{ cm}^2(\text{Vs})^{-1}$ even when their films are deposited at room temperature (RT)

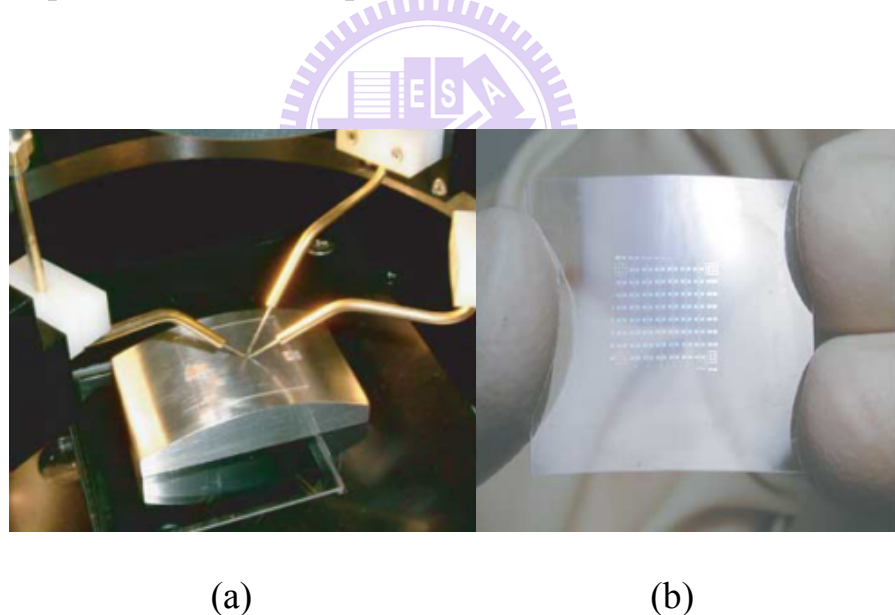


Fig. 1-2 Flexible transparent TFTs (TIFTS) (a) A photograph of the flexible TIFT sheet bent at $R = 30 \text{ mm}$. The TIFT sheet is fully transparent in the visible light range (b) A photograph of the flexible TIFT sheet. The transparent TFT devices are made visible by adjusting the angle of the sheet

illumination²

However, some AOS materials have uncontrollable carriers generated from oxygen vacancy. Therefore, it is important to design and explore a suitable material having both properties of large mobility and stable controllability of carrier concentration for practical applications.

1.2.2. The Carrier Transport Mechanism of AOSs

The mobility of a-Si:H ($\sim 1 \text{ cm}^2(\text{Vs})^{-1}$) is much smaller than that of single crystalline Si ($\sim 200 \text{ cm}^2(\text{Vs})^{-1}$) due to the intrinsic chemical bonding nature. The average carrier transportation paths in covalent semiconductors, such as a-Si:H, consist of strongly directive sp₃ orbitals. The bond angle fluctuation significantly alters the electronic levels, causing high density of deep tail-states, as shown in Fig. 1-3.

In contrast, transparent oxides constituting of heavy post transition metal cations with the $(n-1)d^{10}ns^0$ electron configuration, where $n \geq 5$, are the transparent AOS (TAOS) candidates having large mobilities comparable to those of the corresponding crystals. The electron pathway in oxide semiconductor is primarily composed of spatially spread ns orbitals with an isotropic shape, as shown in Fig. 1-3. The direct overlap among the

neighboring ns orbitals is possible. The degree of overlap of the ns orbitals is insensitive to the distorted metal-oxygen-metal bonding. This feature shows why the Hall mobility of AOSs is similar to the corresponding crystalline phase, even under the room temperature deposition of thin-films.

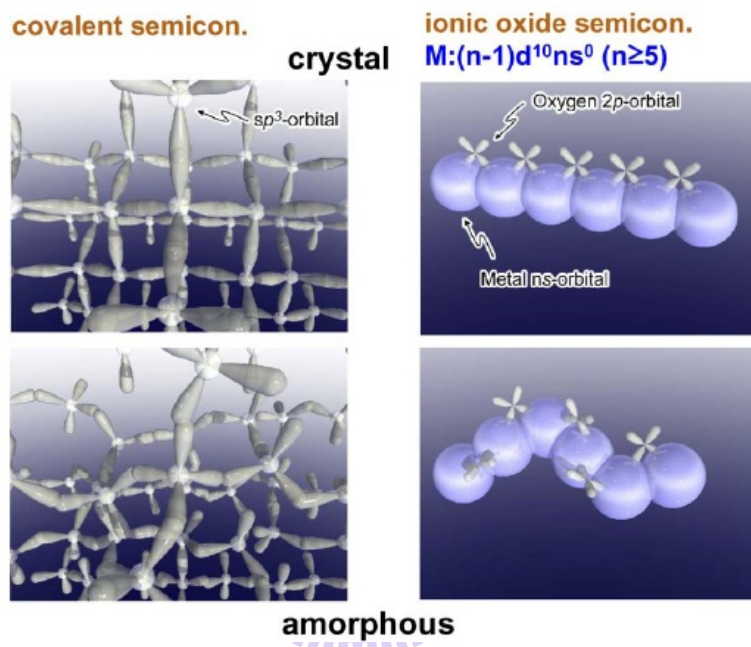


Fig. 1-3 Schematic orbital drawing of electron pathway (conduction band bottom) in conventional silicon-base semiconductor and ionic oxide semiconductor.²

1.3. Amorphous In-Ga-Zn-O TFTs

1.3.1. Introduction

Transparent AOSs have attracted keen attention since the high performance thin-film transistors can be obtained by using the amorphous In-Ga-Zn-O (a-IGZO) thin films for the semiconductor layers deposited on plastic substrates by pulse-laser deposition (PLD) at room temperature.¹ The TFT performance is also confirmed by using the sputter deposition³, which demonstrates the possibility of the large-area applications. The dependence of the TFT characteristics on the metal composition is investigated in detail by a novel combinational approach⁴, since the multi-metal AOSs can take any ratios of the composition.



1.3.2 The $\text{In}_2\text{O}_3\text{-}\text{Ga}_2\text{O}_3\text{-}\text{ZnO}$ Ternary System

For the $\text{In}_2\text{O}_3\text{-}\text{Ga}_2\text{O}_3\text{-}\text{ZnO}$ ternary system, the incorporation of cations with large ionic valance such as Ga^{3+} and Al^{3+} to high conductive oxides such as In_2O_3 and ZnO is effective to control the carrier concentration due to their strong metal-oxygen bonds. Other AOSs, such as a-ITO and c-ZnO have high density carrier density, hence is difficult to control the device characteristics. Besides, amorphous In-Ga-Zn-O (a-IGZO) is transparent throughout the visible spectrum; the transmittance is greater than 80 percent from 400 nm to 850 nm as shown in Fig. 1-4.

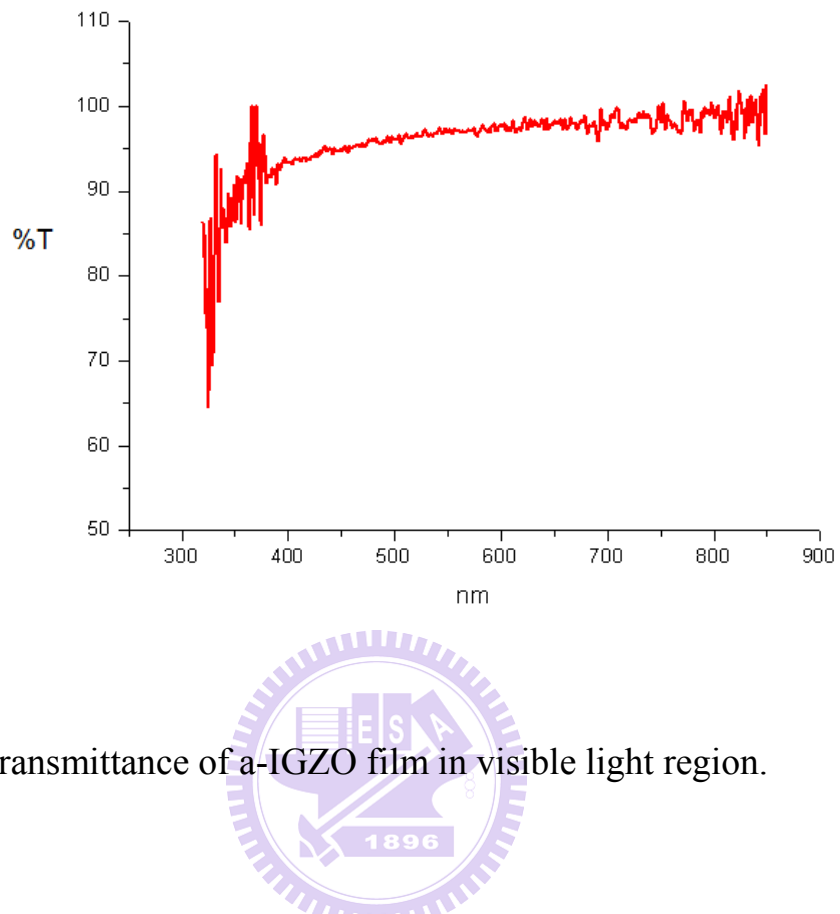


Fig. 1-4 Transmittance of a-IGZO film in visible light region.

The mobility of IGZO is primarily determined by the In_2O_3 content fraction because only In^{3+} meets the electron configuration criterion $(n-1)d^{10}ns^0$ ($n \geq 5$) of heavy post transition metal cation for ionic AOS (IAOS) among the three cations.¹ Fig. 1-5 shows the electron mobilities and concentrations evaluated by the Hall effect measurement for amorphous thin films. The mobility is primarily determined by the fraction of In_2O_3 content and the highest value of $\sim 40\text{cm}^2(\text{Vs})^{-1}$ is obtained for the samples containing the maximum In_2O_3 fraction.

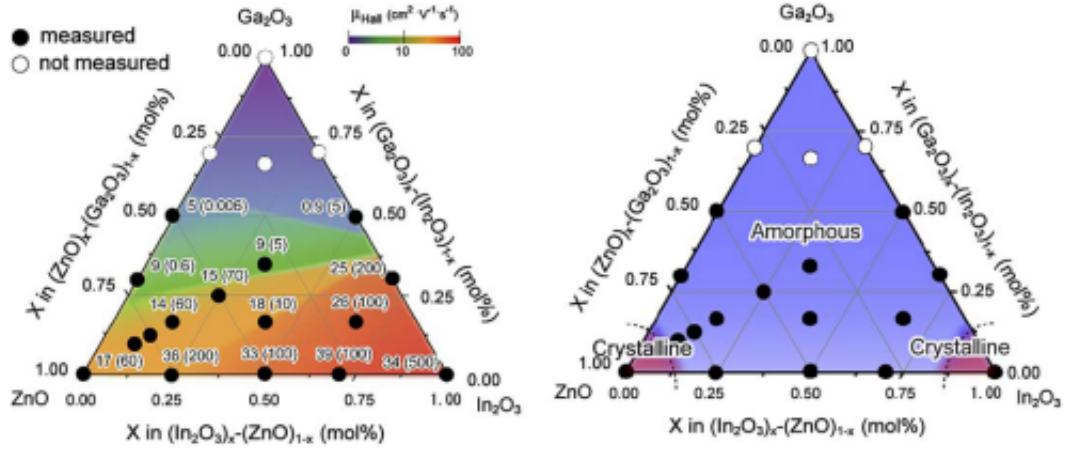


Fig. 1-5 The amorphous formation region (right) and the electron mobilities and concentrations evaluated from the Hall effects for the amorphous thin films (left) in the In_2O_3 - Ga_2O_3 - ZnO system. The thin films were deposited on a glass substrate by PLD under deposition atmosphere of $P_{\text{O}_2} = 1 \text{ Pa}$. Number in the parenthesis denotes carrier electron concentration.¹

The large ionic valence ions such as Ga^{3+} and Al^{3+} combine with high conductive oxides such as In_2O_3 and ZnO to control the carrier concentration effectively because of the strong metal-oxygen bonds. In other words, Ga^{3+} suppresses carrier generation via oxygen vacancy formation because Ga ion forms stronger bond with oxygen than Zn and In ions. Therefore, the InGaZnO_4 composition was chosen as the AOS for channel layer of the transparent TFT.

A critical issue of semiconductor materials for TFT applications is

controllability of carrier concentration. This is particularly important for AOSs because electron carriers can be easily generated. It is vital to choose materials which control carrier concentration at low levels ($\sim 10^{14} \text{ cm}^{-3}$) to achieve low off current (I_{off}) and large on-off current ratio ($I_{\text{on/off}}$). In practice, the effect of binary amorphous materials in the In_2O_3 -ZnO system is employed in commercial flexible transparent conductive films by depositing on plastic sheet. Thus, the effect of partial oxygen pressure was studied on the carrier concentration in a-InGaZnO₄ and a-In₂Zn₃O₆ and the results are shown in Fig. 1-6.

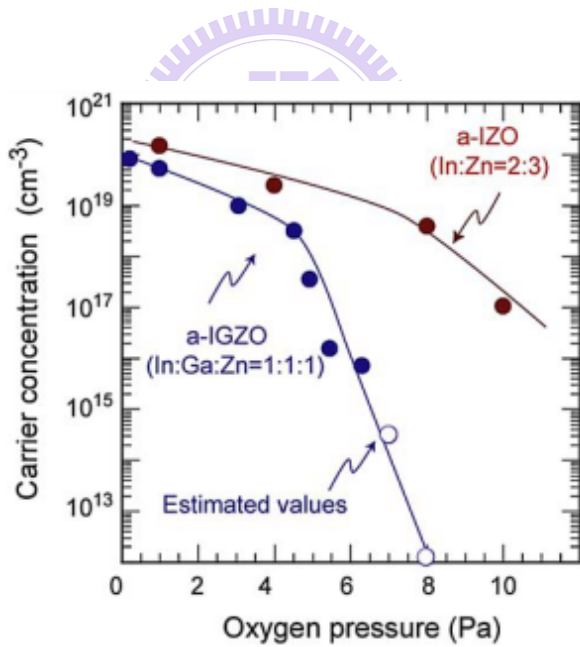
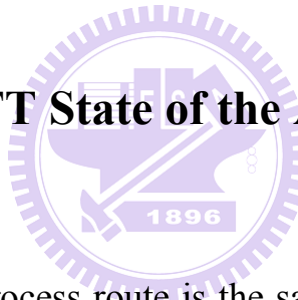


Fig. 1-6 The carrier concentration as a function of O_2 pressure during the deposition in a- InGaZnO₄ and a-In₂Zn₃O₆.¹

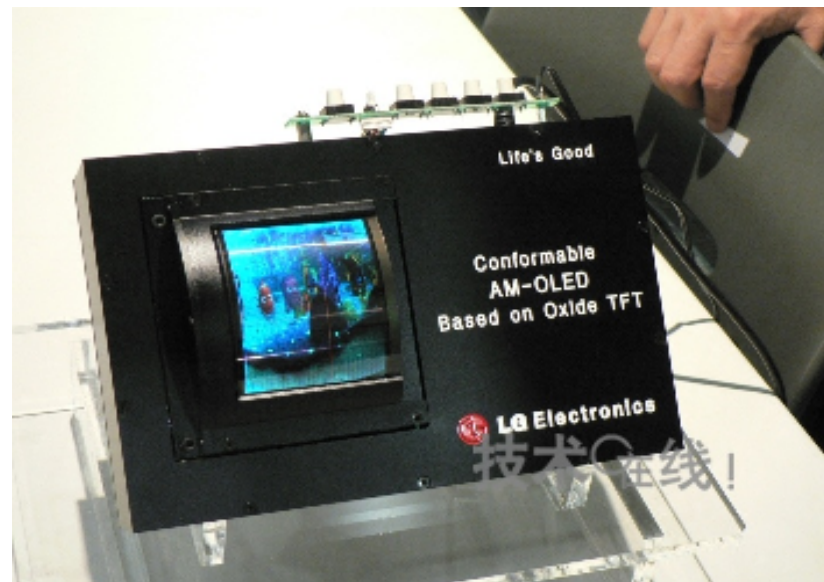
The carrier concentration in the a-InGaZnO₄ is distinctively reduced to

below 10^{13} cm⁻³ by increasing P_{O_2} to 8 Pa, on the other hand, it remains at 10^{18} cm⁻³ in the a-In₂Zn₃O₆ deposited under the same condition. It is evident that incorporation of Ga³⁺ is supposed to attract the oxygen ions tightly due to its high ionic potential (+3 valence and small ionic radius), and thereby suppressing electron injection which is caused by oxygen ion escaping from the thin film. The Hall mobility in the samples around the chemical composition of InGaZnO₄ is not sensitive to the variation in the composition, as shown in Fig. 1-6. Thus, the InGaZnO₄ system has better electrical properties than the In₂Zn₃O₆ system.

1.3.3. The a-IGZO TFT State of the Art



The a-IGZO TFTs process route is the same as a-Si, hence the existing production lines can be used. In 2007, LG Electronics demonstrated a 3.5" AMOLED based on oxide TFT as shown in Fig 1-7 (a). In the same year, Samsung demonstrated a 4" QVGA AMOLED driven by IGZO TFTs, as shown in Fig. 1-7 (b), the mobility of IGZO TFT is $2.6 \text{ cm}^2(\text{Vs})^{-1}$.⁶



(a)

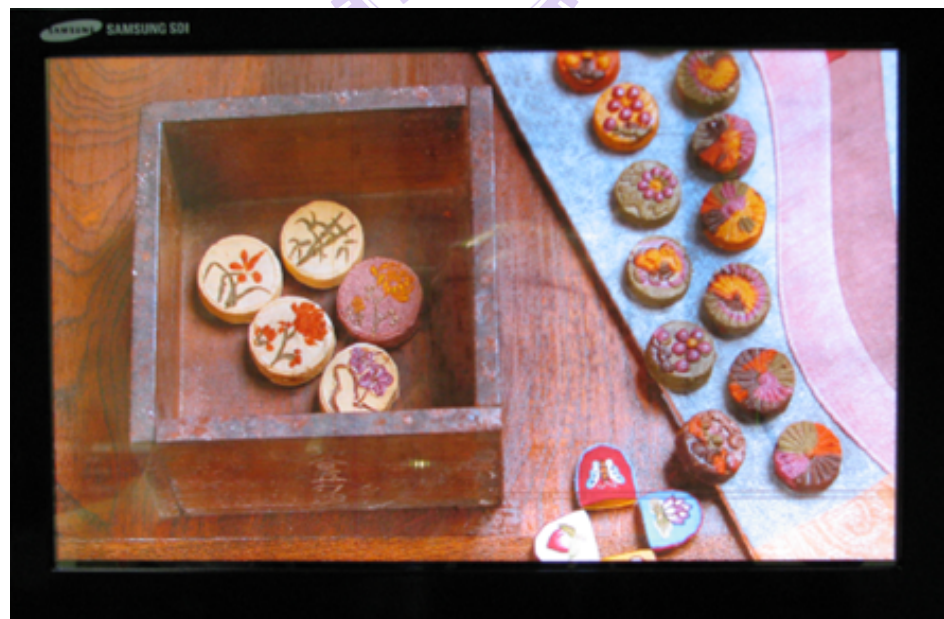
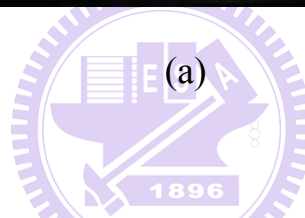


(b)

Fig. 1-7 (a) The display image of LG's 3.5" AMOLED (b) Samsung's AMOLED display driven by InGaZnO TFT

In SID 2008, a full color 12.1 WXGA AMOLED display using a-IGZO

TFTs as an active-matrix backplane was demonstrated by Samsung, as shown in Fig. 1-8.



(b)



(c)

Fig. 1-8 The display image of Samsung's 12.1" WXGA AMOLED display^{6,7}

The a-IGZO TFT exhibited the field-effect mobility (μ) of $8.2 \text{ cm}^2/\text{Vs}$, threshold voltage (V_{th}) of 1.1 V, on /off current ratio of $> 10^8$, and SS of 0.58 V/decade. Besides, the demonstrated AMOLED display was free from the non-uniformity of pixel luminance, which was attributed to the amorphous nature of a-IGZO semiconductor. The AMOLED display with a-IGZO TFT array is promising for large size applications such as HDTV because a-IGZO thin film can be deposited on the large glass substrate (> Gen. 7) by using conventional sputtering system.

1.4. Motivations

The display backplane for large scale and fast switching display is needed.

In my thesis research, a-IGZO TFTs are studied for large scale, high speed TFT backplane. For a-IGZO TFTs, the researches rarely focused on the a-IGZO and gate insulator interface properties and effects of source and drain electrodes. We first study the intrinsic properties of a-IGZO TFTs deposited under different oxygen partial pressure; the effects of post-annealing are also discussed. Second, a dual stack TFT structure is introduced for modifying the a-IGZO and gate dielectric interface properties. Furthermore, the effects of different source and drain electrodes are investigated. This study can be a good reference for the transparent electronic applications.

1.5. Thesis Organization



This thesis is divided into five chapters. In **Chapter 2**, the operation principle of the TFTs is introduced. The measurement and extraction of electrical parameters are also described. The experiments and equipments for a-IGZO TFTs is described in **Chapter 3**. In **Chapter 4**, the electrical properties of a-IGZO films are presented. First, the effects of inlet gas flow ratio and annealing conditions are discussed. Second, the a-IGZO interface conditions and the effects of different source and drain materials on the electrical properties of a-IGZO TFTs are also presented. Finally, conclusions and future works are summarized in **Chapter 5**.

Chapter 2

Principles and Characterizations of TFTs

In this chapter, the principle of TFTs is first introduced. Second, the measurement and the electrical parameter extraction; including threshold voltage, subthreshold swing, field-effect mobility and on/off current ratio are presented. Finally, the surface morphology measurement using the atomic force microscope (AFM) and the contact angle measurement are described.

2.1 Operation Principle of TFTs

Conventional TFTs compose of a semiconductor layer, a gate insulator layer, and three electrode terminals including gate, source and drain. The bottom-gate-top-contact TFT structure is shown in Fig. 2-1.

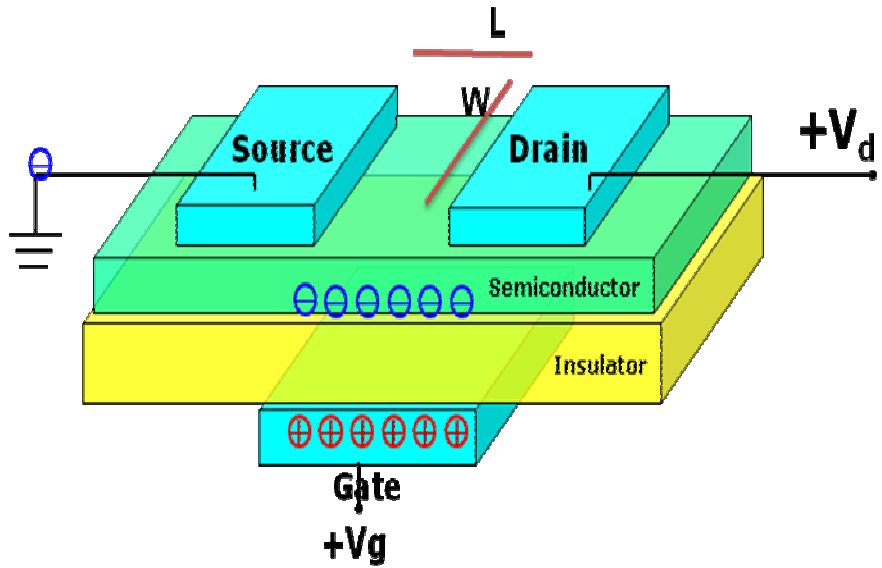


Fig. 2-1 A bottom-gate-top-contact TFT structure.

Transistors can be classified into the depletion-mode and the enhancement-mode, based on whether drain current flows through TFT when no voltage is applied to gate electrode. For the depletion-mode TFT, when the device is on, drain current flows through the device when no gate voltage is applied. For the enhancement-mode TFT, when the device is off, only leakage current flows through the TFT without applying the gate voltage.

The energy band diagrams through the gate of an n-type enhancement-mode TFT is introduced to explain the three modes of TFT operation, as shown in Fig. 2-2.

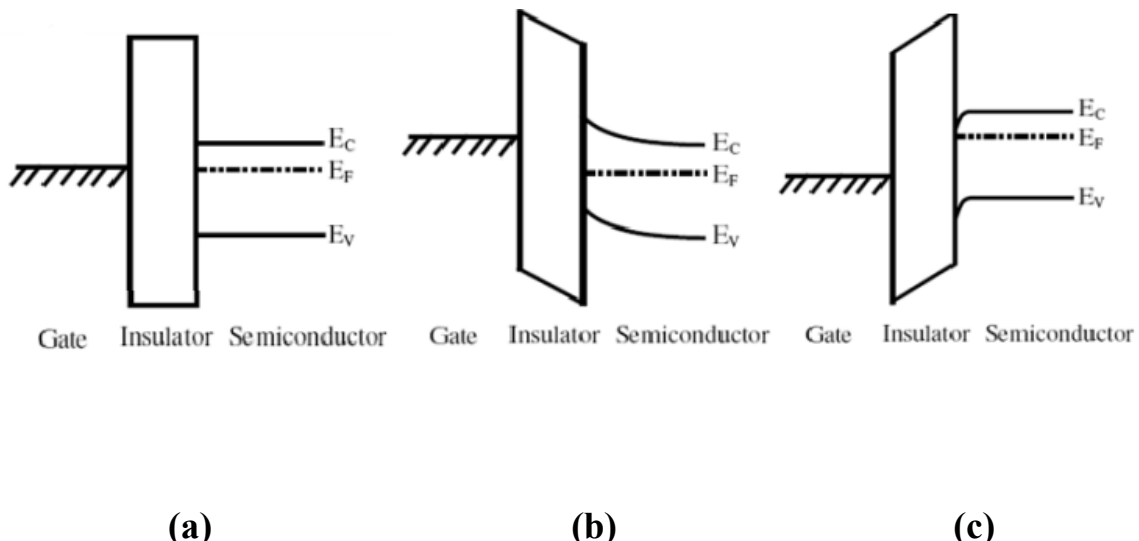


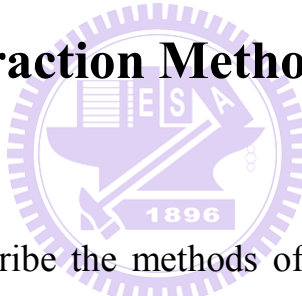
Fig. 2-2 The semiconductor energy band diagram when (a) unbiased, (b) negative gate voltage bias, (c) positive gate voltage bias.

When no gate voltage is applied, the semiconductor is in an equilibrium state. When a negative gate bias is applied, delocalized electrons in the channel are repelled from the semiconductor/gate interface and create a depletion region of positive charge, as indicated by the positive curvature in the conduction band and valance band near the insulator shown in Fig. 2-2 (b). When a positive gate bias is applied, delocalized electrons in the channel are attracted to the semiconductor/insulator interface, creating electron accumulation at the interface, as indicated by the negative curvature in the conduction band and valance band near the insulator in Fig. 2-2 (c). These accumulated electrons at the semiconductor/insulator interface provide a current conduction path and form the channel.

2.2. Electrical Measurement

The device electrical properties were measured by a Keithley 4200 IV analyzer in a light-isolated probe station at room temperature. In I_{DS} - V_{GS} measurement, the typical drain-to-source bias was swept from $V_{GS} = -10$ V to $V_{GS} = 30$ V. In I_{DS} - V_{DS} measurement, the typical drain-to-source bias was swept from $V_{DS} = 0$ V to $V_{DS} = 40$ V.

2.3. Parameter Extraction Method



In this session, we describe the methods of typical parameters extraction such as threshold voltage (V_{th}), subthreshold swing (SS), On/Off current ratio (I_{on}/I_{off}) and field effect mobility (μ_{FE}) from device characteristics.

2.3.1. Determination of the V_{th}

Threshold voltage (V_{th}) was defined from the gate to source voltage at which carrier conduction happens in TFT channel. V_{th} is related to the gate insulator thickness and the flat band voltage.

Plenty of methods are available to determine V_{th} which is one of the most

important parameters of semiconductor devices. This thesis adopts the constant drain current method, that is, the voltage at a specific drain current NI_D is taken as V_{th} , that is, $V_{th} = V_G(NI_D)$ where V_{th} is threshold voltage and NI_D stands for normalized drain current. Constant current method is adopted in most studies of TFTs. It provides a V_{th} close to that obtained by the complex linear extrapolation method. Generally, the threshold current $NI_D = I_D/(W/L)$ is specified at 1 nA in linear region and at 10 nA in saturation region; W and L represent for TFT channel length and width, respectively.

2.3.2. Determination of the Subthreshold Swing



Subthreshold swing (SS, V / dec.) is a typical parameter to describe the control ability of gate toward channel which is the speed of turning the device on and off. It is defined as the amount of gate voltage required to increase and decrease drain current by one order of magnitude. SS is related to the process, and is irrelevant to device dimensions. SS can be lessened by substrate bias since it is affected by the total trap density including interfacial trap density and bulk density. In this study, SS was defined as one-half of the gate voltage required to decrease the threshold current by two orders of magnitude (from $10^{-8}A$ to $10^{-10}A$). The threshold current was specified to be the drain current when the gate voltage is equal to V_{th} .

2.3.3. Determination of the Field-Effect Mobility

Typically, the field-effect mobility (μ_{FE}) is determined from the transconductance (g_m) at low drain bias ($V_D = 0.1$ V). The TFT transfer I-V characteristics can be expressed as

$$I_D = \mu_{FE} C_{ox} \frac{W}{L} [(V_G - V_{th}) V_D - \frac{1}{2} V_D^2] \quad (2-1)$$

Where

C_{ox} is the gate oxide capacitance per unit area,

W is channel width,

L is channel length,

V_{th} is the threshold voltage.



If V_D is much smaller than $V_G - V_{TH}$ (i.e. $V_D \ll V_G - V_{th}$) and $V_G > V_{th}$, the drain current can be approximated as:

$$I_D = \mu_{FE} C_{ox} \frac{W}{L} (V_G - V_{th}) V_D \quad (2-2)$$

The transconductance is defined as:

$$g_m = \mu_{FE} C_{ox} \frac{W}{L} V_D \quad (2-3)$$

Thus,

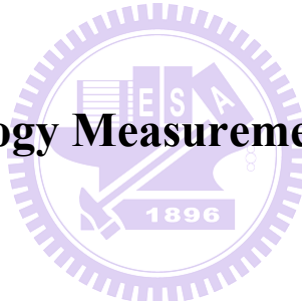
$$\mu_{FE} = \frac{L}{C_{ox} W V_D} g_m \quad (2-4)$$

2.3.4. Determination of On/Off Current Ratio

Drain on/off current ratio is another important factor of TFTs. High on/off current ratio represents not only the large turn-on current but also the small off current (leakage current). It affects AMLCD gray levels (the bright to dark state number) directly.

There are many methods to determine the on and off currents. The practical one is to define the maximum leakage current as off current when drain voltage is applied at 4.5 V.

2.4. Surface Morphology Measurement



The Digital Instruments Dimension 300 atomic force microscope (AFM) was used to characterize the surface morphology of the a-IGZO thin films.

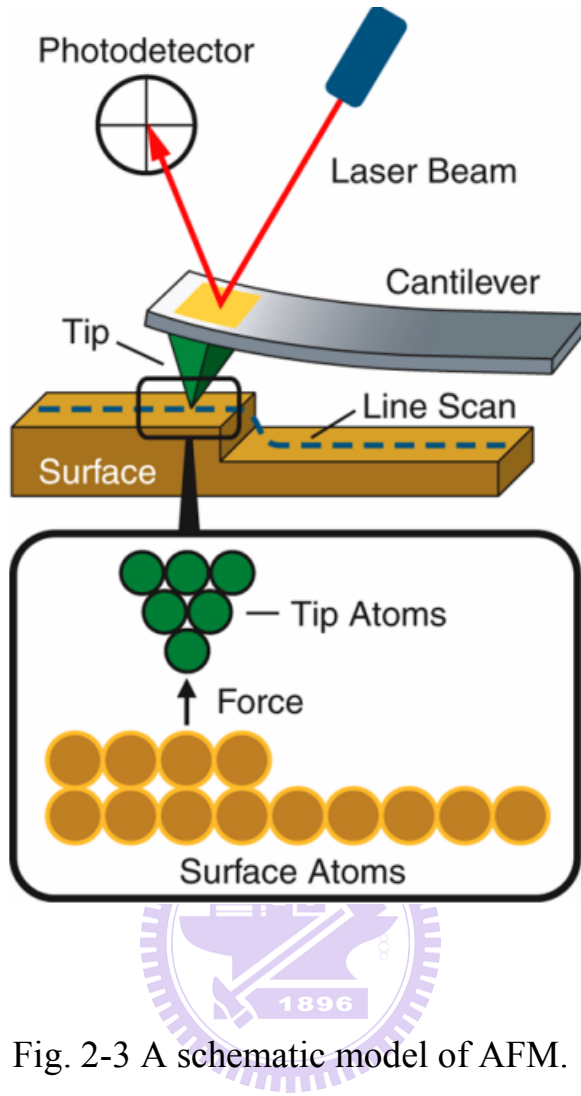


Fig. 2-3 A schematic model of AFM.

The tapping-mode scanning prevents the probe from damaging the sample surface and can get more precise surface topographic information. In the tapping-mode, the probe oscillates up and down regularly. The cantilever vibrates at various frequencies depending on the magnitude of the van der Waals force between the cantilever tip and the sample surface. A laser beam reflected by the cantilever detects the tiny vibration of the cantilever, as shown in Fig. 2-3. The feedback amplitude and the phase signals of the cantilever were recorded by the computer. The amplitude signals provide the morphology information and

the phase signals reveal the material information.

2.5. Contact Angle Measurement

The contact angle is defined by the edge of a liquid droplet on the surface of flat sample; it is formed between the liquid/solid interface and the liquid/vapor interface as illustrated in Fig. 2-4. The static measurement mode is illustrated with a small liquid droplet laying on a flat horizontal solid surface. The static measurement mode is used to estimate wetting properties of a localized region on a solid phase.

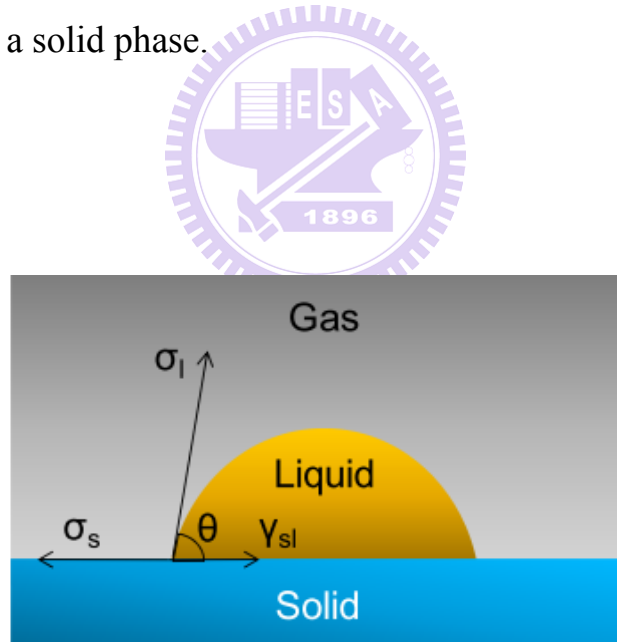


Fig. 2-4 The contact angle formation of liquid on solid surface

The contact angle is specific for any given system and is determined by the interactions across the gas-solid-liquid interfaces. The indices s and l stand for

solid and liquid respectively. The symbols σ_s and σ_l denote the surface tension components of the two phases; the symbol γ_{sl} represents the interfacial tension between the two phases, and θ stands for the contact angle corresponding to the angle between vectors σ_l and γ_{sl} . The relationship between these parameters is the Young's equation ($\sigma_s = \gamma_{sl} + \sigma_l \times \cos\theta$).



Chapter 3

Experimental Methods

The experimental methods of the fabrication of the a-IGZO TFT are described. Besides, the principle of sputtering system including the RF sputtering and the DC sputtering, is described,

3.1. a-IGZO TFT Device Fabrication

(1) Substrate Cleaning



The detail sequence to clean the n^+ heavily doped silicon (Si) is:

Step 1: Clean Si wafer by DI water for 3 mins

Step 2: Clean Si wafer by DHF solution for 10 seconds

Step 3: Use N_2 purge to dry the Si wafer; place them into a glass container with a cover.

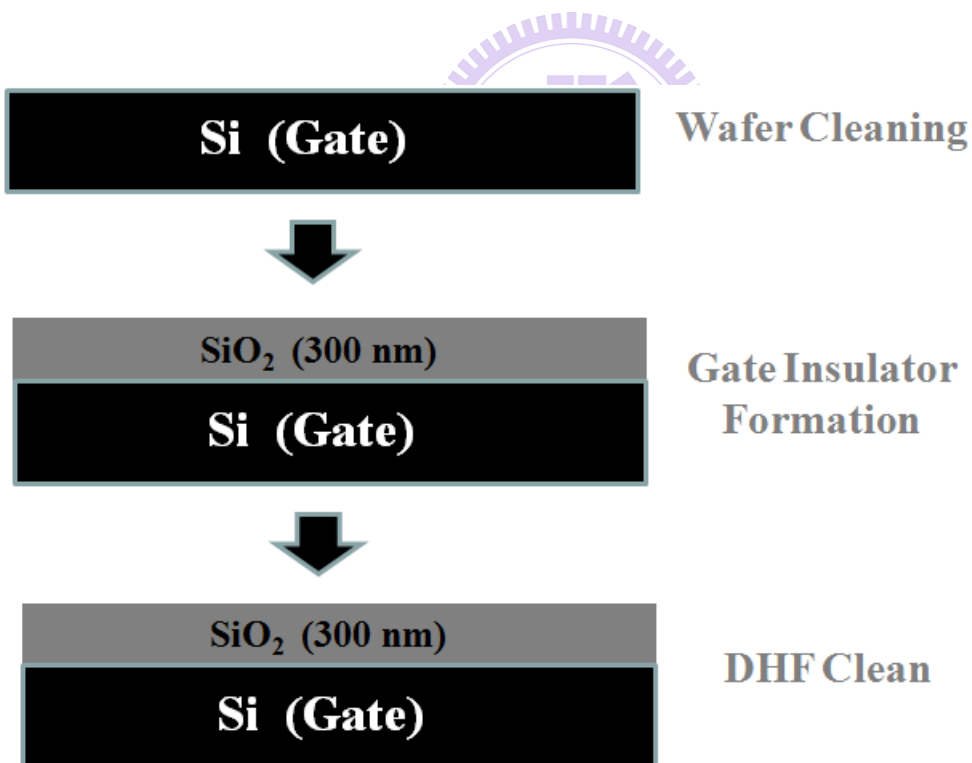
Step 4: Put the glass container into an oven at $100^\circ C$ for 1 min

(2) Preparation of Gate Insulator Layer

A 300 nm thick silicon oxide (SiO_2) for the gate dielectric was thermally grown in the horizontal furnace by using the low pressure chemical vapor deposition (LPCVD) method. A high quality insulator is required in order to suppress the gate leakage current.

(3) Device Processing Steps

A typical a-IGZO TFT processing flow chart is shown below.



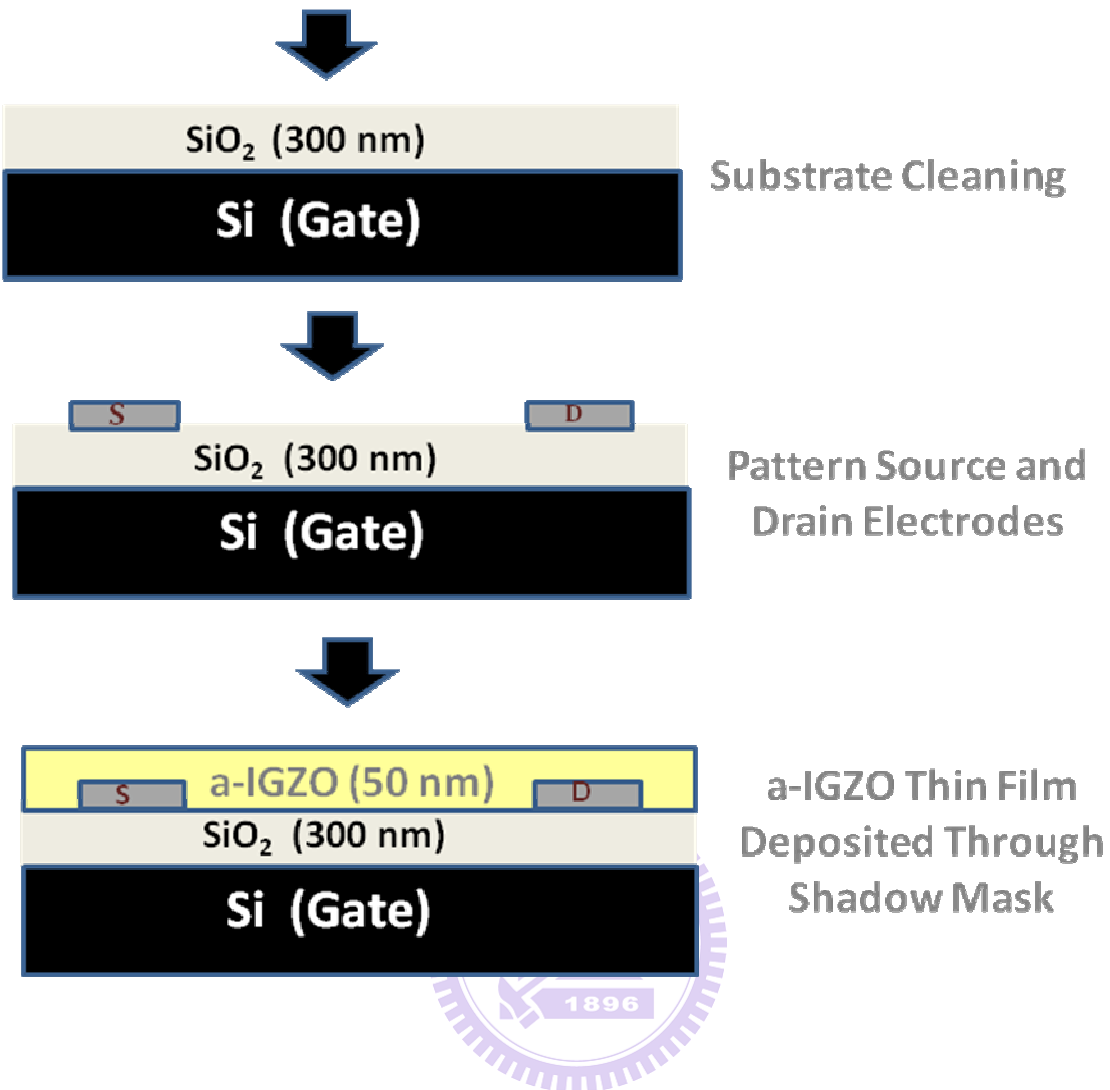


Fig. 3-1 The flow chart of typical a-IGZO TFT device fabrication

Fig. 3-1 shows the preparation of the bottom gate a-IGZO TFT structure used in this study. A heavily doped (N^+) prime Si wafer with 300 nm thermal oxide layer was selected as the gate electrode and insulator, respectively. Following, the 40 nm thick source and drain electrodes were deposited through stencil mask openings. The deposition methods for different source and drain are shown in Table 3-1. Finally, a 50 nm thick a-IGZO (In:Ga:Zn = 1:1:1) thin-film was deposited by sputter at room temperature. The RF sputtering was

used for reducing the charges accumulated on the a-IGZO target. The deposition was done with a continuously gas flow of argon and oxygen without intentional substrate heating.

Table 3-1 The electrode fabrication methods.

	Au	Ti	Al	ITO
Depositing Method	Thermal Evaporation	E-gun Evaporation	Thermal Evaporation	Sputter

Finally, the devices were thermally-annealed by a tube furnace in the nitrogen atmosphere at 350°C for defect elimination. In the nitrogen atmosphere at high temperature. Oxygen molecules with only partial bonding on the a-IGZO thin film surface will outgas, and the semiconductor characteristics can be improved.

The channel width (W) of the device were of 600 μm and the channel lengths (L) are 200, 400, 600, 800 or 1000 μm .

Electrical measurement of the a-IGZO TFT was carried out with a probe station system located in a light tight box. The electrical properties of TFTs were measured by a PC controlled Keithley 4200 semiconductor parameter analyzer. For measuring the TFT transfer characteristics, the drain-to-source voltage (V_{DS}) was changed in between 1 and 11 V. The gate-to-source voltage

(V_{GS}) was varied from -10 V to 30 V. All measurements were done at room temperature in ambient air.

3.2. Sputtering

3.2.1. RF Sputtering

RF sputtering can be applied to the deposition of both insulating and conducting materials. Figure 3-2 shows a RF sputtering system, the substrate is located above the target so that the sputtered atoms can be deposited on to the substrate. A RF power supply generates plasma at the frequency of 13.56 MHz. The plasma creates ions which are accelerated towards the target by a negative DC bias on the target. The ions bombard the target surface and dislodge the target atoms, which then deposit onto the substrate. The sputtering is performed in vacuum, typically between 1 mTorr and 50 mTorr. A lower chamber pressure increases the mean free path, which is the distance between collisions, so that the sputtered target atoms can reach the substrate without scattering away.

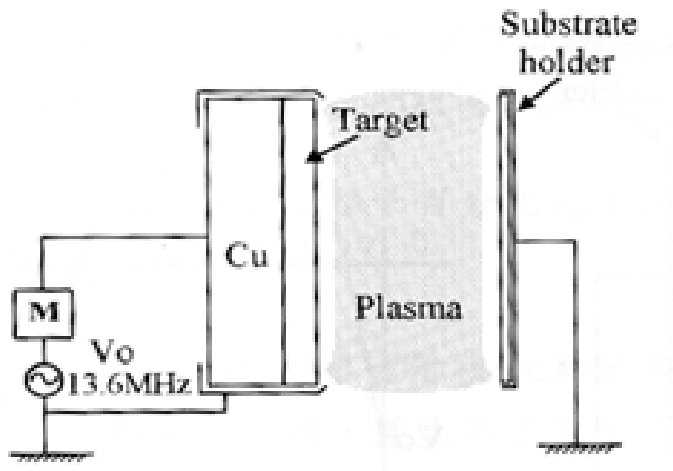


Fig. 3-2 Schematic RF sputtering system.

3.2.1. DC Sputtering



DC sputtering has the advantage of higher deposition rate and is less expensive than RF sputtering. A DC sputtering system is shown in Fig. 3-3, the substrate is located above the target and acts as the anode. DC sputtering is commonly applied to deposit conductive materials.

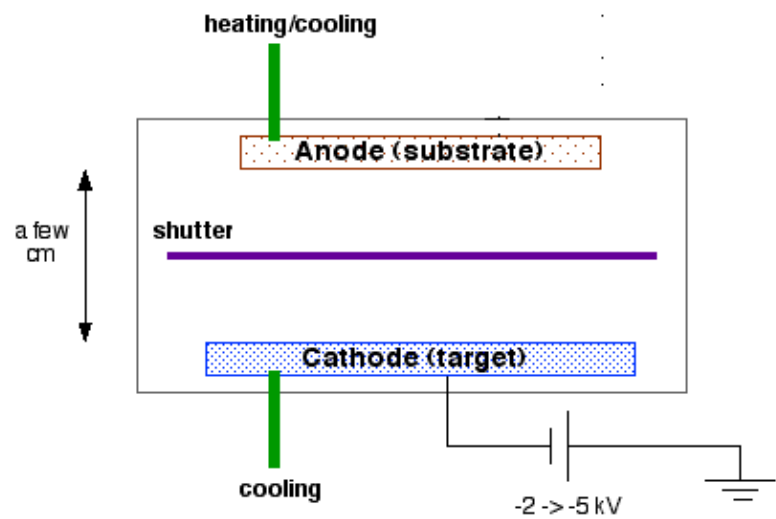
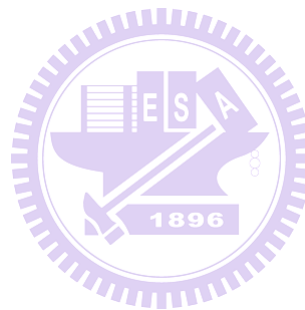


Fig. 3-3 Schematic DC sputtering system.



Chapter 4

Results and Discussion

4.1. The Effects of Oxygen Flow Rate and Post-Annealing on a-IGZO TFTs

4.1.1. Introduction



The carrier source of Si and metal oxide is shown in Fig. 4-1. For Si, the carriers are resulted from impurity doping as shown in Fig. 4-1 (a). Electrons dominate the carrier transport for phosphorous-doped Si. Carrier transport is dominated by holes for boron-doped Si. For metal oxide, the carrier concentration is related to the oxygen vacancy; one oxygen vacancy provides two electrons, as shown in Fig. 4-1 (b).

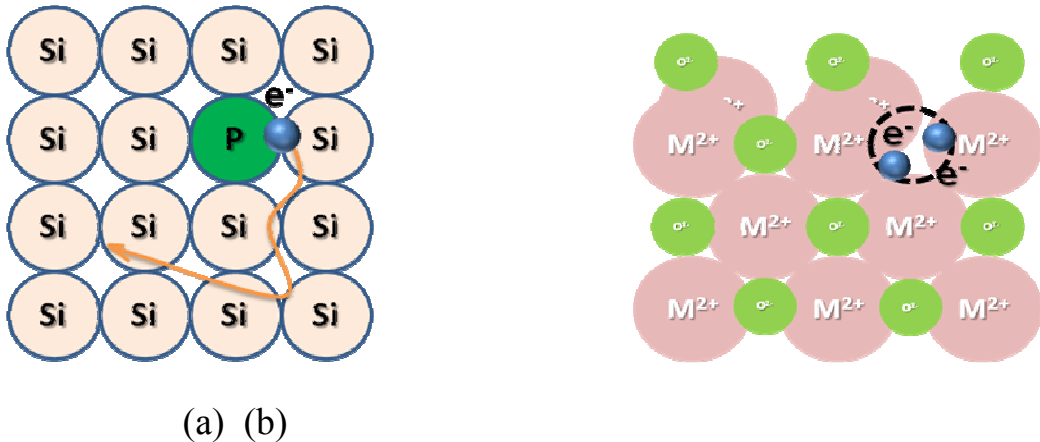


Fig. 4-1 The carrier source of (a) Si, (b) Metal oxide.

Because of the oxygen vacancies in the a-IGZO film, a-IGZO TFT characteristics are strongly associated with the a-IGZO film. The reactions on film surface dominate the threshold voltage (V_{th}) shift. The oxygen absorption changes the carrier concentration. The oxygen absorption forms depletion layer, resulting in V_{th} shift.

The oxygen absorption accompanies partial charge transfer, V_{th} varies at different oxygen flow rate implies the change in carrier concentration during the absorption and desorption processes. When the oxygen flow rate increases, the channel carrier concentration decreases because of less oxygen vacancies in a-IGZO film. Therefore, higher voltage is needed to turn on the channel.

The electrical characteristics of IGZO film can be controlled by varying the deposition conditions (Ar flow rate and O₂ flow rate). When the oxygen flow rate is low, IGZO film is not applicable for TFT channel layer because the film

conductivity is high. When oxygen flow rate is high (over 8 sccm), IGZO film becomes insulator. In intermediate oxygen flow rate (5~8) sccm, IGZO shows semiconductor characteristics and is suitable for channel layer. It is considered that the low oxygen flow rate increases the electrical conductivity of the deposited film.^{1,5} In the case of Ar gas flow, even though it is not strongly related to electrical property of IGZO film, it is one of the key parameter to control the uniformity of TFT behavior. Fig. 4-2 shows that only in a proper range of P_{O_2} will the a-IGZO exhibit the semiconductor characteristics.⁴ In our experiments, several oxygen flow rates (0 sccm, 0.2 sccm, 0.4 sccm, 0.6 sccm, 0.8 sccm) were adopted so as to prepare the a-IGZO TFTs with various electrical characteristics.

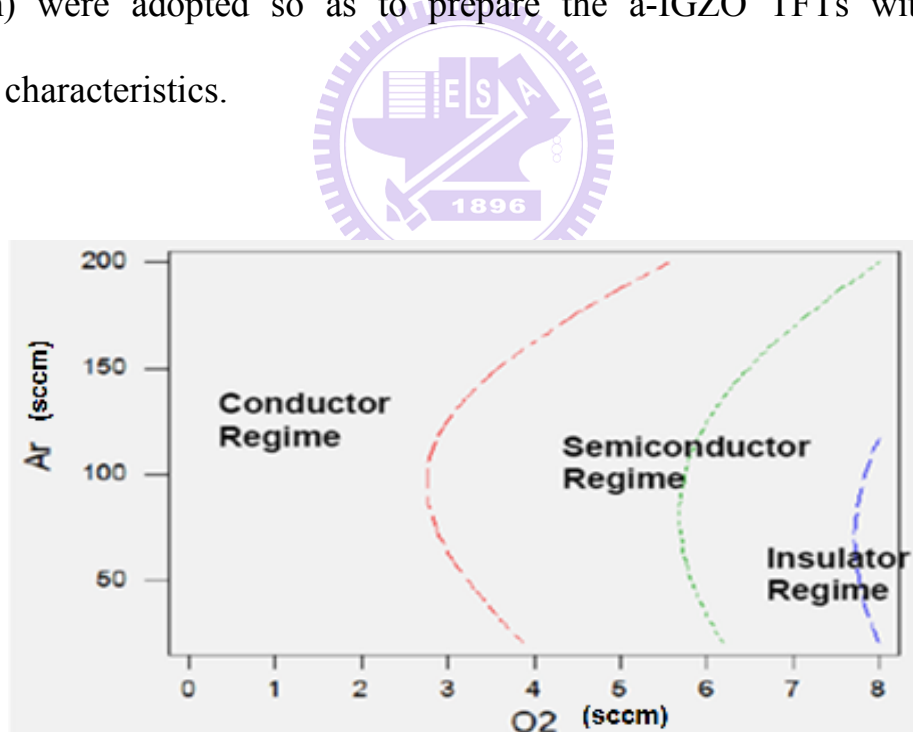


Fig. 4-2 Electrical property of IGZO TFT as a function of oxygen and argon flow rate during deposition.⁶

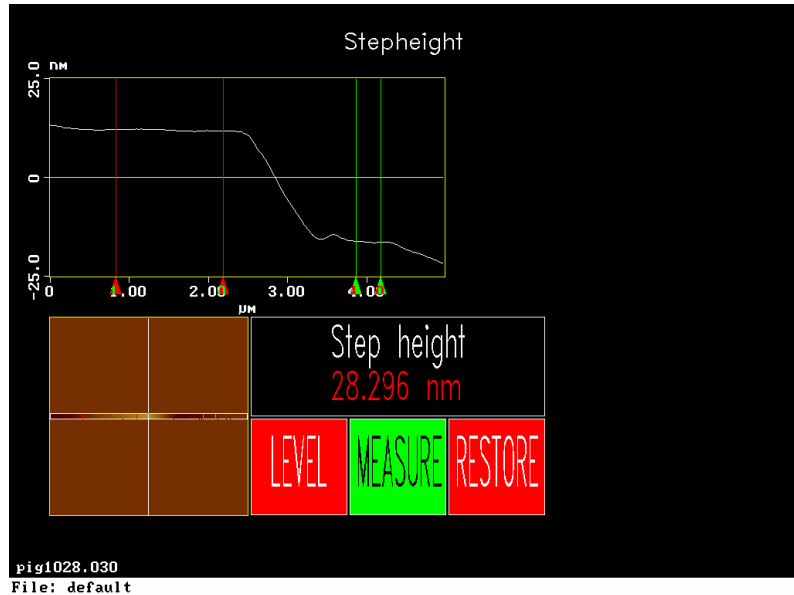
4.1.2. Results and Discussion

4.1.2.1. Determination of the Deposition Rate

First, the deposition rate of IGZO was determined by measuring the film thickness with the AFM. The AFM results of a-IGZO film thickness are shown in Fig. 3-3. The deposition rate is about 5.933 nm/min for oxygen flow rate = 0 sccm device and 3.537 nm/min for oxygen flow rate = 0.6 sccm device.



(a)



(b)

Fig. 4-3 The AFM result of (a) 0 sccm O₂ device deposited for 6.5 mins.
(b) 0.6 sccm O₂ device deposited for 8 mins

4.1.2.2. The Effects of Oxygen Flow Rate on a-IGZO TFTs

The a-IGZO TFTs were operated in enhancement mode. The SiO₂ gate insulator is 100 nm thick and the post-annealing time is 1.5 hours. Good electrical characteristics like large on-state drain current, small threshold voltage, and low threshold voltage were obtained when the oxygen flow rate is 0 sccm, as shown in Fig.4-4.

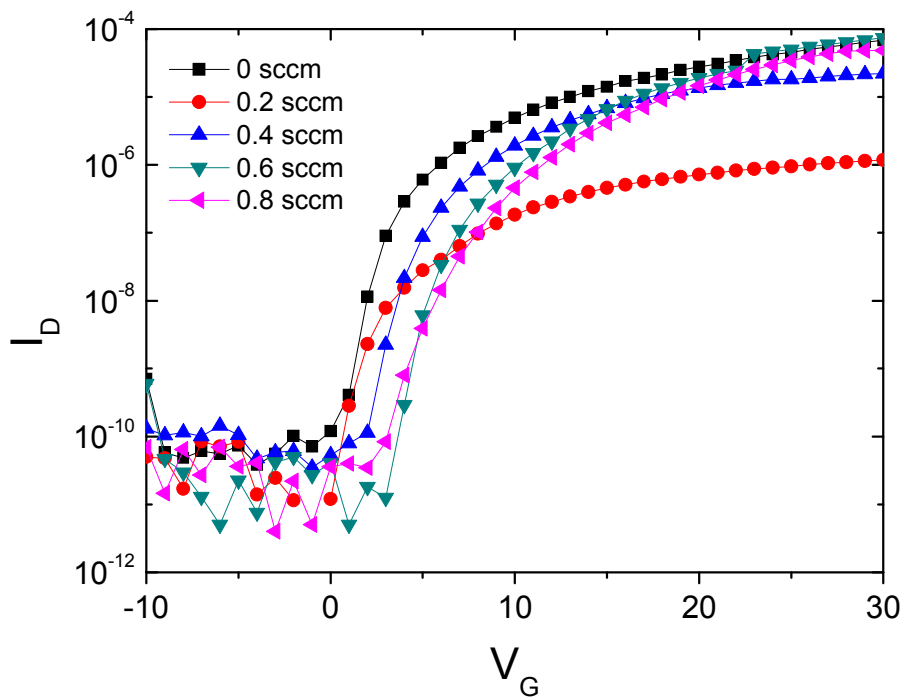
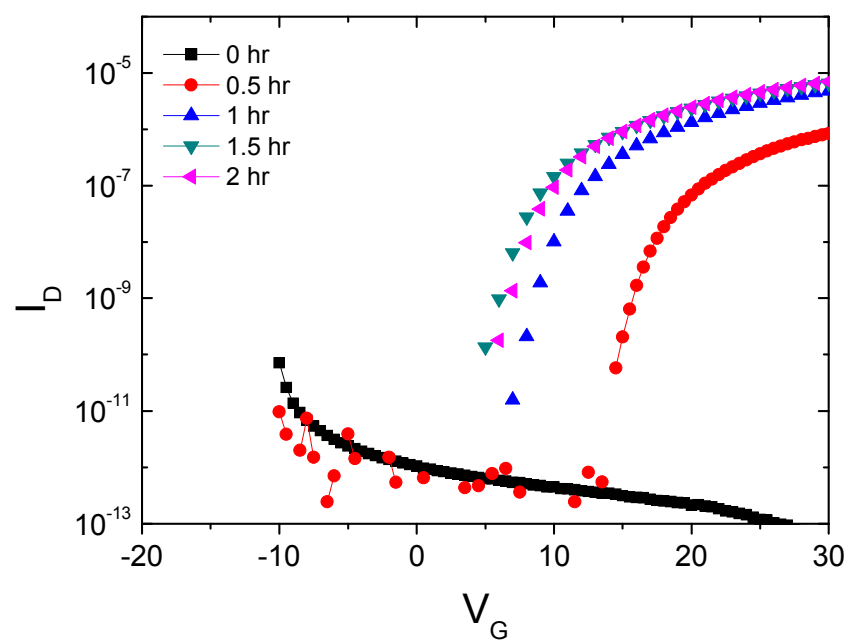
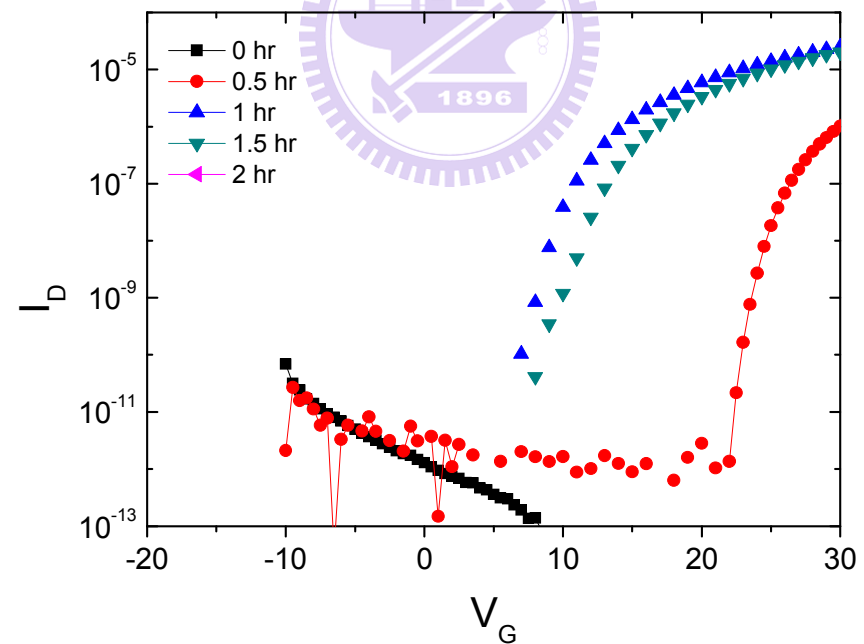


Fig. 4-4 The a-IGZO TFT output characteristics for different oxygen flow rates.

As a result, under the same post-annealing time, V_{th} is smaller for smaller oxygen flow rate. The decrease of V_{th} is due to the mobile carrier increase. The mobile carrier increase in channel relates to the oxygen flow rate and affects the channel/dielectric interface by changing the density of interface states. In other words, less oxygen vacancies are filled when the oxygen flow rate is smaller. The oxygen vacancies provide electrons and increase the channel carrier concentration, leading to a smaller V_{th} .



(a)



(b)

Fig. 4-5 Annealing 0 to 2 hours of O_2 flow rate (a) 0 sccm, (b) 0.6 sccm.

4.1.2.3. The Effects of Post-Annealing on a-IGZO TFTs

TFT based on AOSs (e.g. IGO ZTO, ZIO) sputtered in pure Ar requires high annealing temperature ($T > 300$ °C) to exhibit satisfactory electrical characteristics; including better saturation current, smaller hysteresis, and V_{th} .

The post-annealing effects on device with 300 nm SiO_2 gate insulator is shown in Fig. 4-5. V_{th} shifts negatively after post-annealing because post-annealing leads to the lattice structure rearrangement, structural relaxation, and the improved a-IGZO bonding. Post-annealing improves the channel/dielectric interface; and the charge trapping defects are decreased.

The electrical output characteristics for devices post-annealed for 2 and 3 hours are compared in Fig. 4-6. Annealing causes modification of the semiconductor/insulator interface, local atomic rearrangement and improved bonding. Three-hour annealing is the appropriate for a-IGZO TFT with a 300 nm SiO_2 gate insulator. V_{th} shifts negatively to be near 0 V after the thermal treatment.

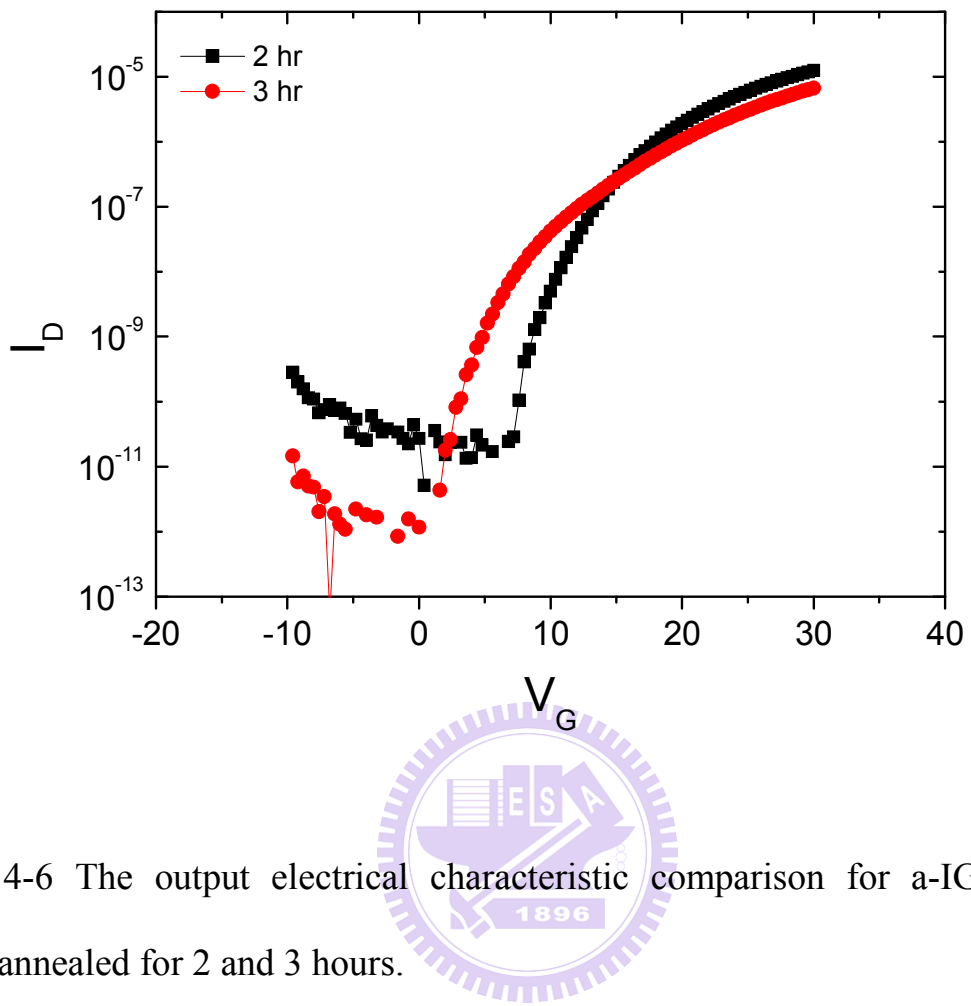


Fig. 4-6 The output electrical characteristic comparison for a-IGZO TFTs post-annealed for 2 and 3 hours.

4-1-3. Conclusions

The oxygen flow rate was varied to examine oxygen absorption effect. The V_{th} changes with the oxygen flow rate. The oxygen vacancies provide electrons and increase the channel carrier concentration, leading to a smaller V_{th} .

Post-annealing improves the crystallinity in a-IGZO because of the semiconductor/insulator interface modification and local atomic rearrangement and the threshold voltage can be adjusted to be near 0 V.

It is found that IGZO thin film transistors are very sensitive to oxygen and can be used as oxygen or pressure sensors.⁹

4.2. The Interface Modification for a-IGZO TFTs

4.2.1. Introduction

Research for a-IGZO TFT was focused on the intrinsic limitations of semiconductor. A large V_{th} is still an issue for a-IGZO TFT. It is noteworthy that a high interface trap density at the semiconductor/dielectric interface increases the V_{th} . A large V_{th} leads to the “hard saturation” phenomena in the electrical output characteristics. Besides, a poor dielectric layer quality leads to the increase of gate leakage current.

In this session, the a-IGZO TFT with the dual-stack structure is introduced, as shown in Fig.4-7. A buffer layer and the gate dielectric insulator were stacked up. The buffer layer is an interface modification layer. The buffer layer materials used in this study were hafnium oxide (HfO_2), aluminum oxide (Al_2O_3), and hexamethyldisilazane (HMDS). Device with only the SiO_2 gate insulator is for comparison.

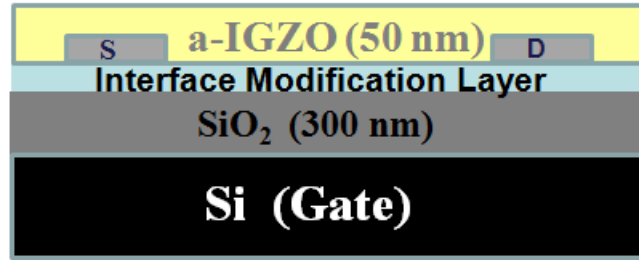


Fig. 4-7 The dual stack a-IGZO TFT structure.

The HfO₂ and Al₂O₃ buffer layers are both 10 nm thick, and are deposited by the e-gun evaporation on SiO₂ for the a-IGZO/gate dielectric surface treatment, as shown in Fig. 4-7. The series capacitance of the SiO₂/buffer layer was dominated by the thicker 300nm SiO₂ and the contribution of the thinner buffer layer was estimated to be of less than 10 %.

4.2.2. Result and Discussion

The buffered-TFT output characteristic comparison is shown in Fig. 4-8. It is noticeable that I_D of the HMDS-buffered a-IGZO TFT is increased.

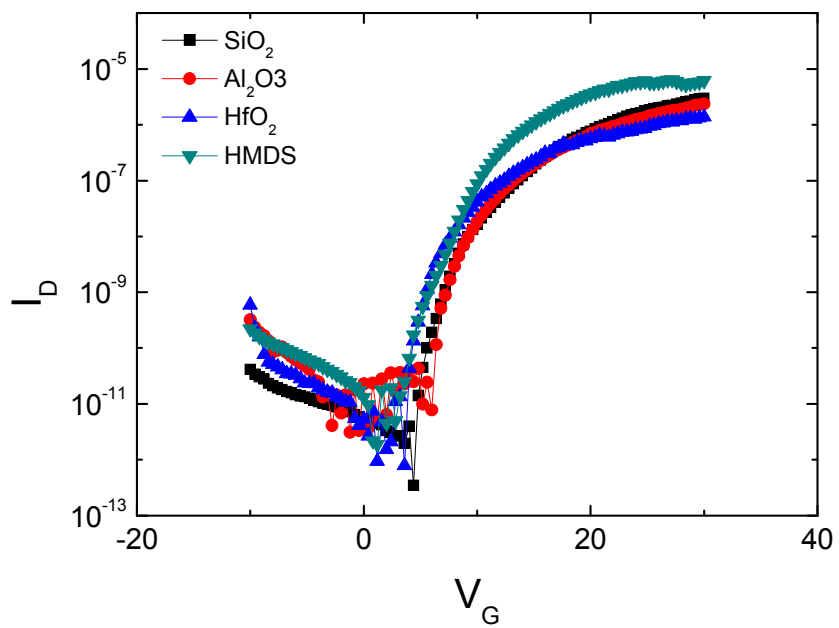


Fig. 4-8 I_D - V_G curve comparison of the buffered-a-IGZO TFTs.

The contact angle measurement result is shown in Fig. 4-9. The water drop on HMDS has the largest contact angle on the HMDS surface, indicating that a-IGZO has improved interfacial condition when it is stacked with a hydrophobic material.

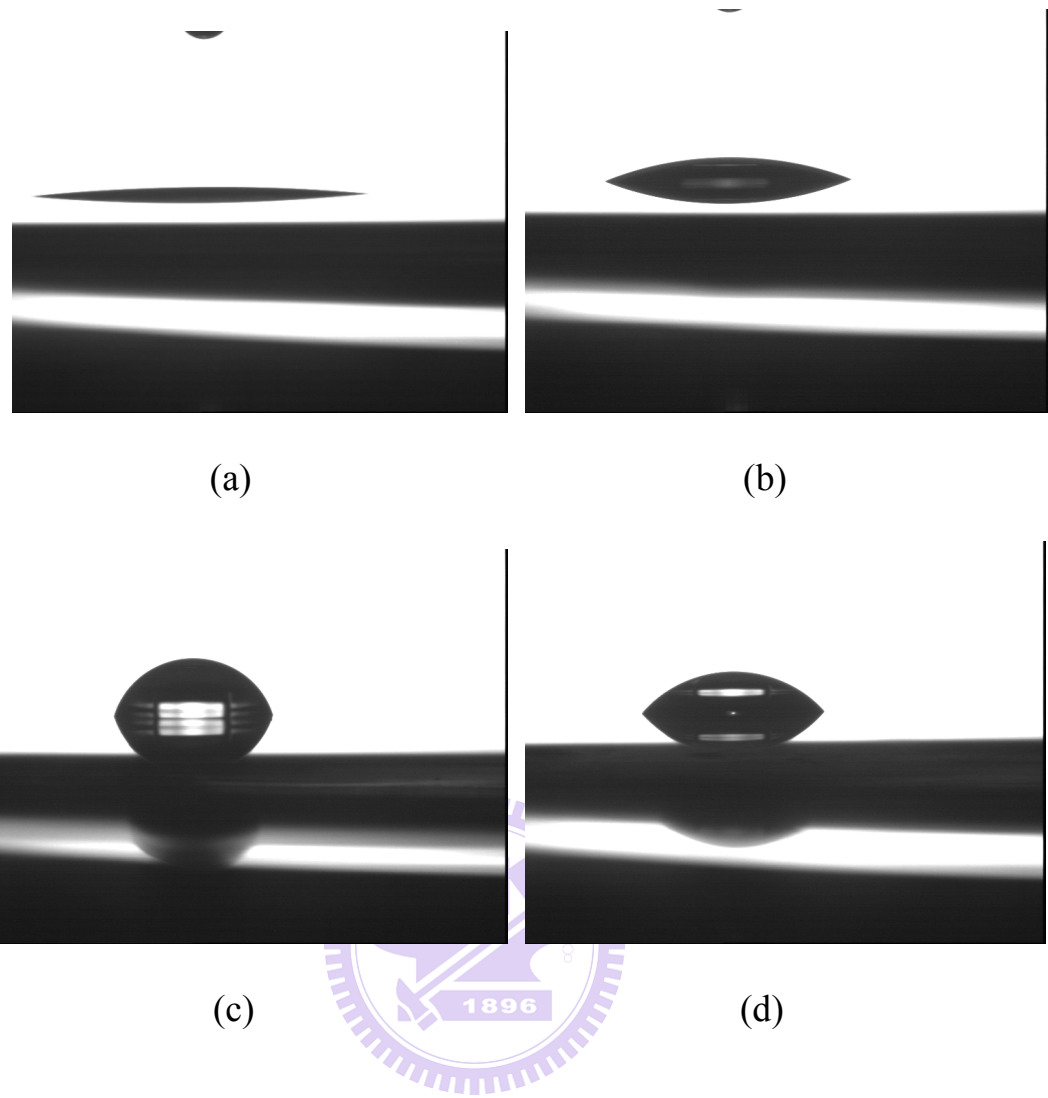


Fig 4-9 Contact angle image for water drop on the
 (a) Al_2O_3 , (b) HfO_2 , (c) HMDS, and (d) SiO_2 surface.

Table 4-1 Contact angle of different buffer layer surface.

	Al_2O_3	HfO_2	SiO_2	HMDS
CA-left(°)	5.21	21.55	47.64	72.46
CA-right(°)	5.21	21.55	47.64	72.46

The performance comparison of a-IGZO TFT with the interface modification layer is shown in Table 4-2. The mobility of the HDMS-buffered TFT was enhanced to $13.67 \text{ cm}^2/\text{Vs}$.

Table 4-2 The performance of the a-IGZO TFTs with the interface modification layer.

	Mobility (cm^2/Vs)	V_{th}	S.S.
SiO_2	6.79	9.05	0.59
Hf_2O_3	7.81	9.24	0.69
Al_2O_3	6.87	7.68	0.62
HMDS	13.67	7.76	0.64



4.2.3. Conclusion

A dual stack TFT structure is introduced to examine the properties of the a-IGZO/gate insulator interface. The interface modification materials adopted in this session are HfO_2 , Al_2O_3 , and HMDS. As a result, HMDS improves the field-effect mobility of the a-IGZO TFT. All buffered-TFTs have higher mobility than TFT without the interface modification, indicating that the gate insulator/active layer interface is improved.

From the contact angle measurement; HMDS surface has the largest contact angle for the water drop, indicating that a-IGZO has improved interfacial condition when it is stacked with hydrophobic material HMDS.

The proposed dual layer structure has shown a great potential for the advanced AMLCD technology since the output electrical characteristics of a-IGZO TFTs are greatly related to the conditions of the a-IGZO semiconductor/gate insulator interface.

4.3. The Effects of Source and Drain Electrodes on a-IGZO TFTs

4.3.1. Introduction

The unmatched source/drain electrodes lead to the high series contact resistance, causing the current suppression phenomena. Furthermore, a high contact resistance induces the current crowding effect and increases the V_{th} . Thus, a high efficient contact is necessary to attain electrical properties.

For a-Si:H TFTs, the source to drain resistance is influenced by the contact resistance between n+ a-Si:H and the source/drain metal; by the bulk resistance

of the n+ a-Si:H film, by the interface effect between n+ a-Si:H and source/drain electrodes, and by the intrinsic a-Si:H layer sheet resistance.

Unlike a-Si:H TFTs, the proposed a-IGZO TFT does not have a highly doped ohmic layer, the source to drain resistance is affected by the interface properties between intrinsic a-IGZO and the source/drain metal. These properties are the interface trap, the effective contact area, and the barrier height and width between the a-IGZO semiconductor and the source/drain metal.

Compared to a-Si:H TFT, the a-IGZO TFT source to drain resistance is more dependent on the channel resistance, because the interface properties are related to the gate voltage.



In our study, the a-IGZO TFTs were fabricated using materials with different work function for the source/drain electrodes. These materials are as follows: titanium (Ti), gold (Au), aluminum (Al), and indium-tin-oxide (ITO), which is widely used in a-IGZO TFT researches. The chosen electrode materials are widely used not only in the integrated circuit (IC) industry but also in the display applications.

First, the effect of different source and drain electrodes on a-IGZO TFT is investigated. Following, the effect of ambient interactions on a-IGZO TFT without passivation is discussed.

4.3.2. Results and Discussion

4-3-2-1. The Effects of Source/Drain Electrodes on a-IGZO TFTs

The I_D - V_G characteristics of a-IGZO TFTs with different source/drain electrodes are shown in Fig. 4-10. The a-IGZO TFT with Ti source/drain electrodes has the highest on-state current (I_{on}) and the smallest V_{th} .

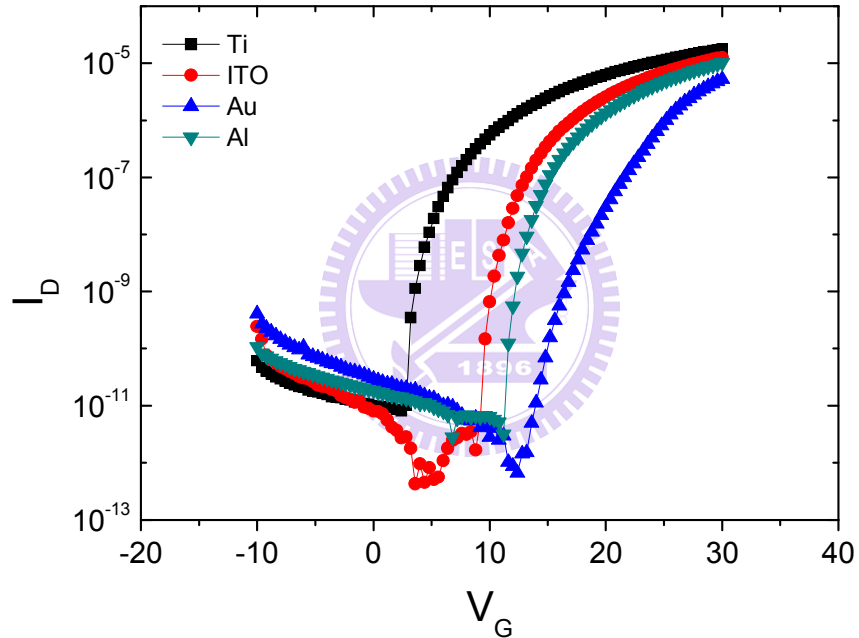


Fig. 4-10 The electrical characteristics comparison for a-IGZO TFTs with different source/drain electrodes.

The a-IGZO TFT output characteristics can be related to the work function difference between the a-IGZO semiconductor and the source/drain electrodes. The work functions of several metallic materials are shown in Fig. 4-11. As a

result, Ti has the lowest V_{th} and Au has the highest V_{th} .

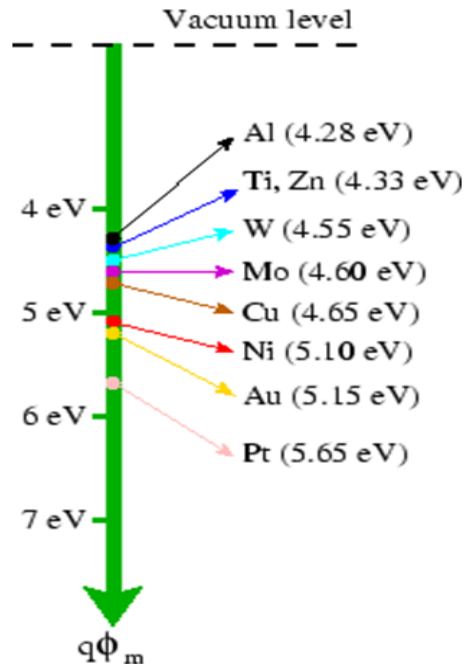
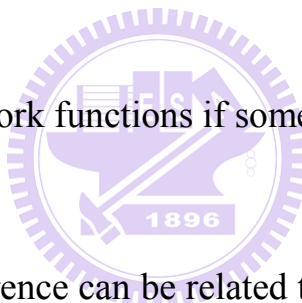


Figure 4-11 The work functions of some metallic materials.



The work function difference can be related to the contact resistance. The larger the work function difference, the larger the contact resistance. Figure 4-10 shows the contact resistances (R_c) of various source/drain materials. Generally, Au has the highest R_c , Al has larger R_c than ITO. Ti provides the lowest R_c , indicating that Ti provides the smallest work function difference between the source/drain materials and the a-IGZO thin film.

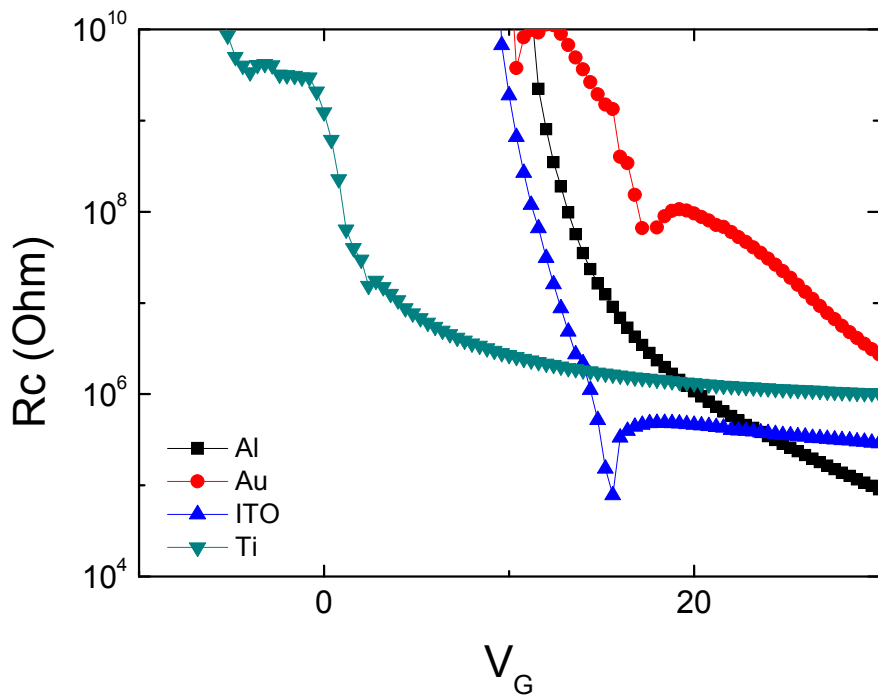


Fig. 4-12 The contact resistance comparison for different source/drain electrodes.



The method adopted for extracting R_c is as shown below:

For linear region drain current formula:

$$I_D = (W/L)\mu C_{ox}(V_G - V_t)V_D$$

Partial differential to drain voltage was taken:

$$\partial I_D / \partial V_D = (R_{\text{total}})^{-1}$$

$$R_{\text{total}} = R_c + R_{\text{ch}}$$

If under the same V_G , with two different lengths a and b:

$$R_{ta} = R_c + aK \dots(1)$$

$$R_{tb} = R_c + bK \dots(2)$$

$$(2) \times a/b \dots(3)$$

From (1) – (3), R_c was obtained.

The comparison for a-IGZO TFT output electrical characteristics with varied source/drain is shown in Table 4-3. A large work function difference between channel and electrodes leads to a large Schottky Barrier and increases V_{th} . As a result, Au has the largest threshold voltage because Au has the largest contact resistance for a-IGZO film. In other words, a large contact resistance causes the current crowding effects, leading to a large V_{th} . On the other hand, a large contact resistance increases the Schottky Barrier and reduces mobility. In our experiments, for Al, Au, Ti, ITO, the different source/drain electrode materials, the mobilities of a-IGZO TFTs are appropriate for display applications. As a result, the a-IGZO TFT with the Ti source/drain electrodes has high μ , the lowest V_{th} , and the smallest SS. Therefore, Ti is an appropriate source/drain material for the high performance a-IGZO TFT.

Table 4-3 Electrical properties comparison for varied electrodes.

	μ (cm ² /Vs)	V _{th} (V)	S.S. (V/dec)
Ti	11.77	4.65	0.58
ITO	10.07	11.3	0.63
Au	12.31	20.17	2.22
Al	10.05	13.24	0.58

4.3.2.2. The Ambient Effects on a-IGZO TFTs

The a-IGZO film is sensitive to the surface absorption of oxygen and water molecules. When the oxygen molecules in atmosphere fill into the oxygen vacancies, they decrease the electrical conductivity of a-IGZO film. In other view, the oxygen vacancies can be assumed as holes and they can assist the electrical conduction of a-IGZO film. Therefore, the filling of oxygen vacancies reduces the electrical conduction of a-IGZO film. On the other hand, there are also oxygen molecules carrying electrons in ambience. They also fill in to the oxygen vacancies, affecting electrical characteristics.

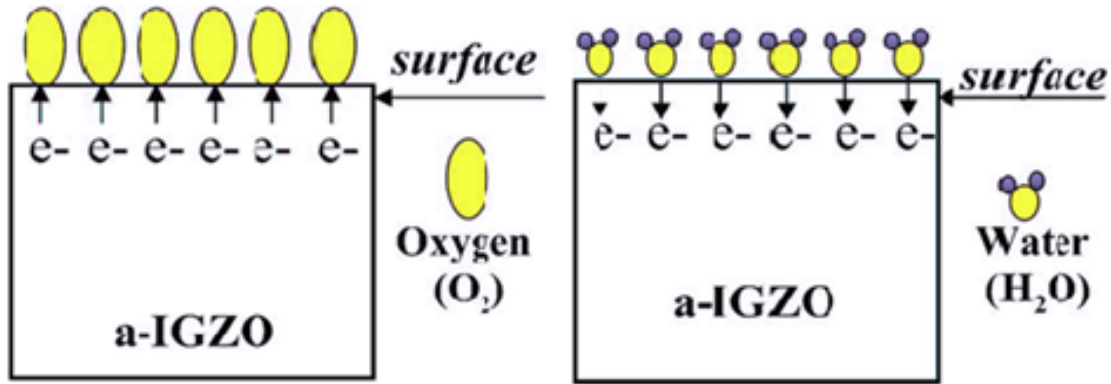
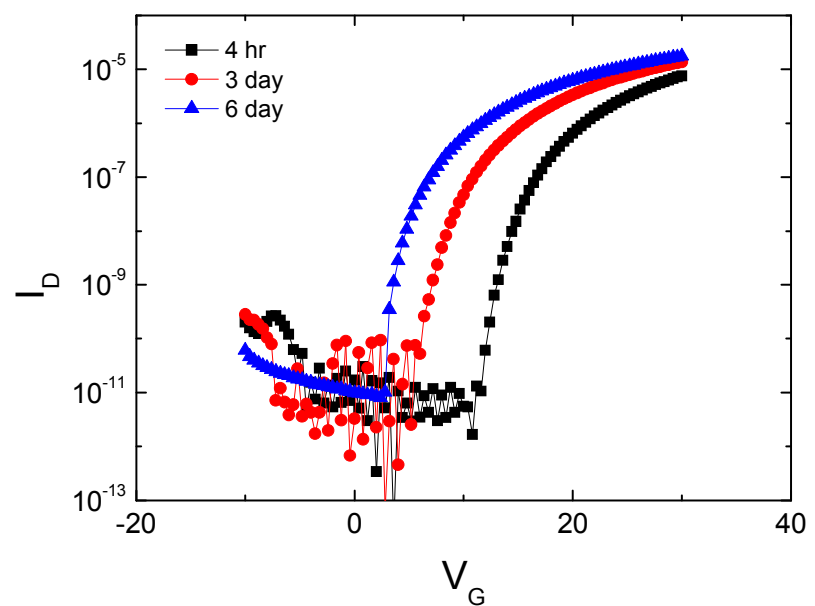
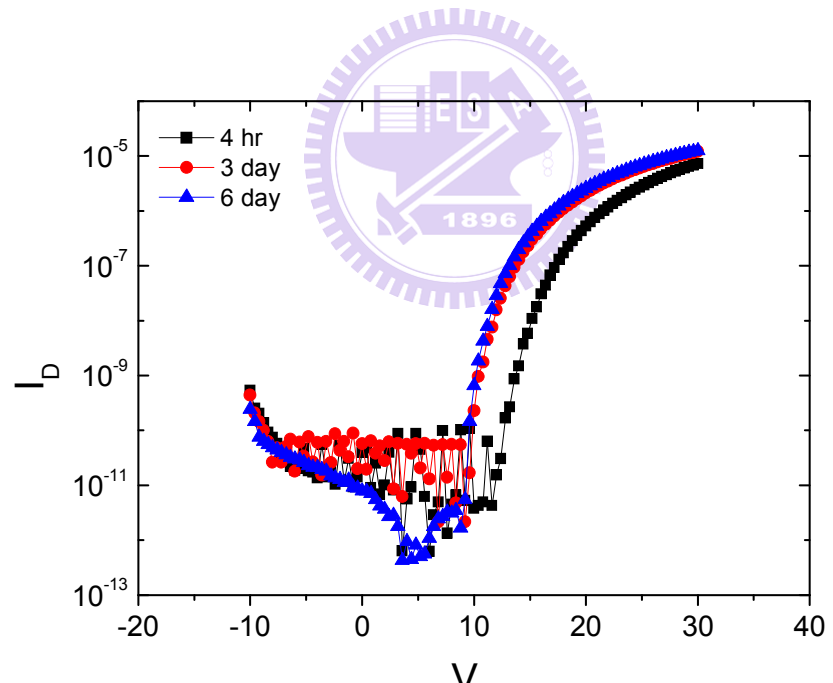


Fig. 4-13 The schematic diagram showing the role of (a) oxygen as an electron acceptor and (b) water molecules as a electron donor onto a-IGZO surface.¹⁴

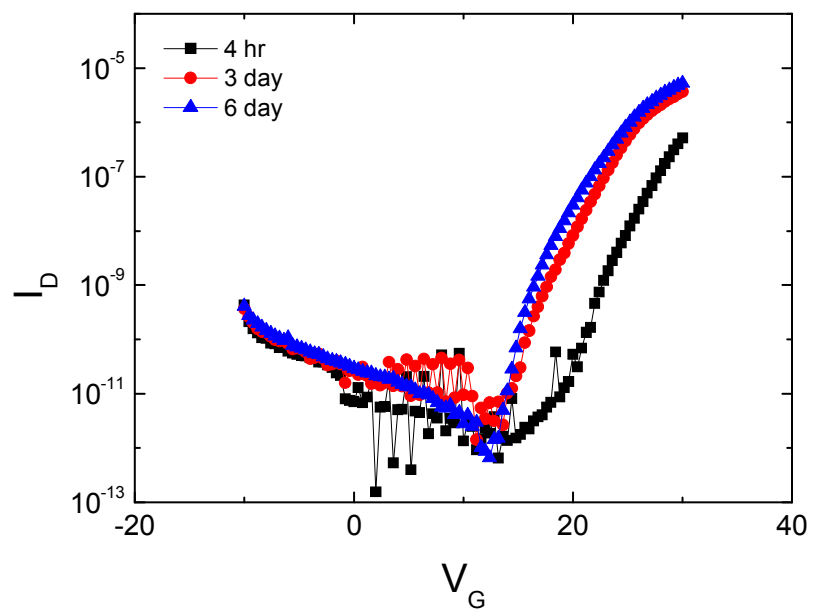
The shift of the V_{th} over time for a-IGZO TFTs with different source/drain electrodes is shown in Fig. 4-13. For a-IGZO TFT, the water molecule absorption is the main cause for the shift of threshold voltage. The oxygen molecules are absorbed on both channel and electrodes, but are electrically active only on channel. In atmosphere, the metastable hole traps form in oxide semiconductors. The water molecules diffuse in and out a-IGZO film adversely affects a-IGZO properties.¹³



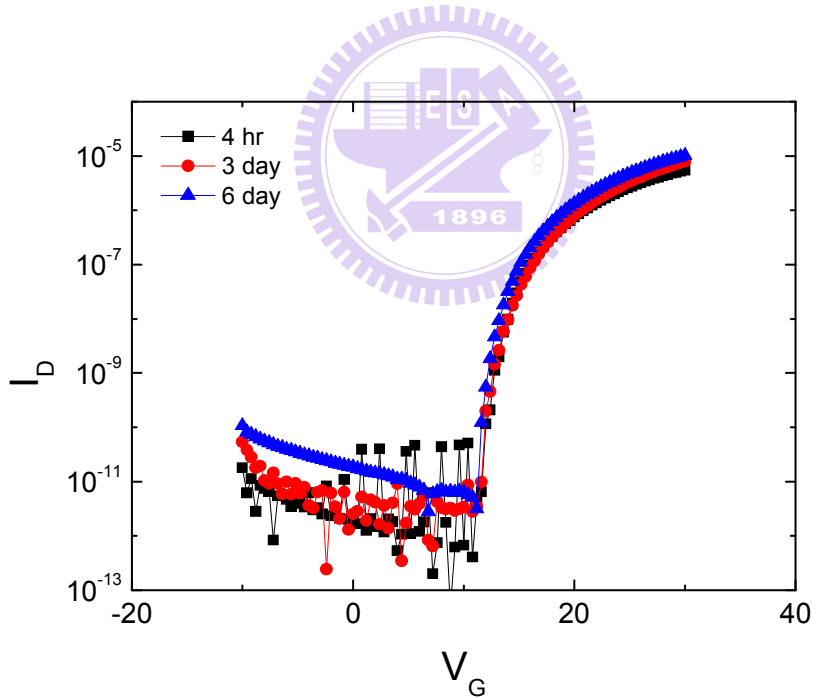
(a)



(b)



(c)



(d)

Fig. 4-14 The negative shift of the threshold voltage over time for a-IGZO TFT with (a) Ti, (b) ITO, (c) Au, and (d) Al source/drain electrodes

The absorbed oxygen molecules undergo the partial charge transfer, and form the depletion layer below the a-IGZO active layer surface, hence shifts the threshold voltage positively.

On the other hand, the water molecules on a-IGZO surface act as the electron trapping centers.¹³ The water molecules absorbed by a-IGZO film form the accumulation layer below the a-IGZO film surface, hence shifts the V_{th} negatively. The surface interactions on a-IGZO thin film with the water molecules involves the trap creation/removal in active layer. As a result, the negative V_{th} shift was observed, indicating that in atmosphere, the interaction with water molecules is the dominant mechanism for a-IGZO TFT.



4.3.3. Conclusions

The a-IGZO TFTs with varying source/drain materials, which are Ti, Au, Al, and ITO, were fabricated without passivation for investigating electrical performance of the a-IGZO TFT.

First, the output electrical characteristics for a-IGZO TFTs with different source/drain electrodes were compared. The work function difference between a-IGZO active layer and the source/drain electrodes can be considered as the

contact resistance. The larger the work function difference between a-IGZO thin film and the source/drain electrodes leads to the larger contact resistance. The contact resistance is related to the mobility and the threshold voltage. In our experiments, a-IGZO TFT with Au source/drain electrodes has the largest contact resistance. As a result, the higher contact resistance leads to the higher mobility because of the higher carrier injection efficiency. On the other hand, the higher work function difference induces the current crowding effect, leading to the larger threshold voltage. The a-IGZO TFT with Ti source/drain electrodes has the lowest contact resistance; and the device performance is appropriate for the display applications.



Second, since the a-IGZO device without passivation interacts with the atmosphere, the ambience effects were investigated. The oxygen molecules form the electron trapping centers on the a-IGZO surface, thus reduce the carrier concentration. In contrast, the absorbed oxygen molecules deplete electrons while water molecules induce the electron accumulation layer. The water molecule absorption donates the partial electron transfer to the a-IGZO film surface. The water molecule absorption dominates the a-IGZO surface interaction in ambience. As a result, the threshold voltage shifts negatively.

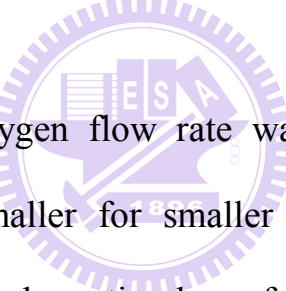
Therefore, the adoption of the passivation layer prevents the degradation under humidity. Passivation is the key factor for sustaining the a-IGZO TFT subthreshold properties and the devices reliability.

Chapter 5

Conclusion

5.1. Conclusions

We report on the properties of a-IGZO TFTs fabricated on Si substrate at room temperature using sputtering process.



In the first part, the oxygen flow rate was varied to examine oxygen absorption effect. V_{th} is smaller for smaller oxygen flow rate, since the depletion layer underneath the absorption layer forms due to the charge transfer between absorbed O_2 and a-IGZO forms.

Post-annealing improves the crystallinity in a-IGZO because of the semiconductor/insulator interface modification and local atomic rearrangement. As a result, the field mobility can be up to $11.42 \text{ cm}^2(\text{Vs})^{-1}$ and the threshold voltage can be adjusted to be near 0 V. Our device performance is appropriate for display applications.

In the second part, the dual stack a-IGZO TFT structure is introduced to

examine the properties of the a-IGZO/gate insulator interface. The interface modification materials adopted are HfO_2 , Al_2O_3 , and HMDS. HMDS greatly improves the field-effect mobility of the a-IGZO TFT. As a result, HMDS-buffered a-IGZO TFT has larger mobility, implying improved channel/dielectric interfacial condition when it is stacked with the hydrophobic material HMDS.

In the third part, the effects of different source/drain materials on a-IGZO TFT were investigated. The adopted materials are Ti, Au, Al, and ITO.

First, the contact resistance is related to the mobility and the threshold voltage. The higher contact resistance leads to the lower mobility while the higher work function difference leads to the larger threshold voltage. The performance of the a-IGZO TFT with Ti source/drain electrodes is appropriate for the display applications.

Second, since the a-IGZO device without passivation interacts with the atmosphere, the ambience effects were investigated. The oxygen molecules reduce the carrier concentration. In contrast, the water molecule absorption provides electrons. The water molecule absorption dominates the a-IGZO surface interaction in ambience and the threshold voltage shifts negatively.

5.2. Future Work

Recently, the issue of the threshold voltage shift for a-IGZO TFT is a hot topic for fabricating a-IGZO TFT backplane for display application. The Canon's proposed devise structure on SID' 08, as shown in Fig. 5-1.

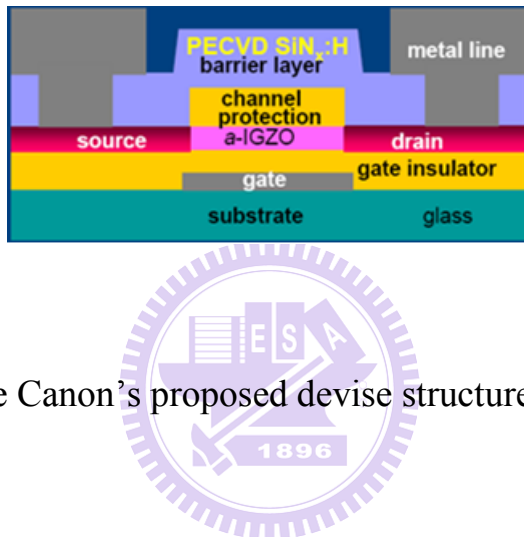


Fig. 5-1 The Canon's proposed devise structure on SID' 08.

However, in our future work, the direct Si_3N_4 passivation on a-IGZO by the PECVD process will not be adopted since the hydrogen doped Si_3N_4 will increase the a-IGZO conductivity, as shown in Fig. 5-2.

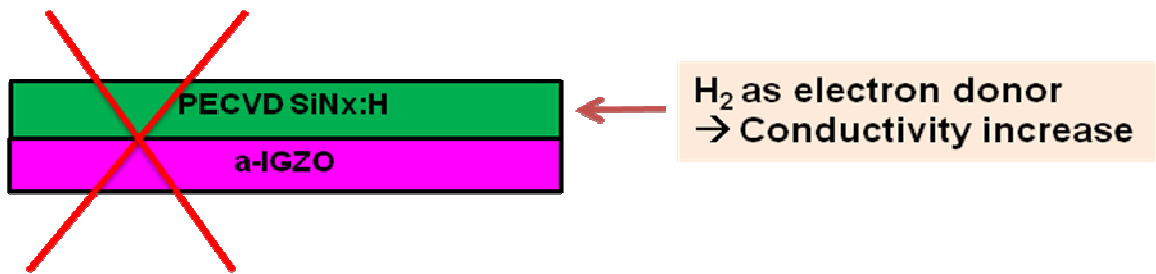


Fig. 5-2 The a-IGZO layer with the Si_3N_4 passivation layer.

In our proposed TFT structure with passivation layer, an oxygen rich SiO_2 channel protection layer on the a-IGZO thin film can prevent a-IGZO from losing the O_2 . A Si_3N_4 layer can further suppress the active layer surface interaction with the ambience, as shown in Fig. 5-3.

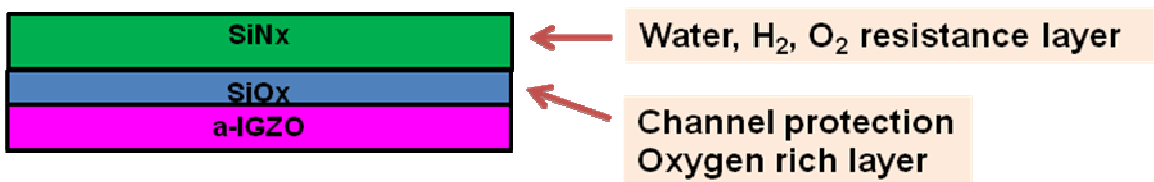


Fig. 5-3 The proposed structure for a-IGZO passivation.

In addition, the comparison for organic/inorganic passivation will be further studied and discussed. Ink-jet printing technology will be utilized to process organic materials into TFT devices.

The adoption of the passivation layer prevents the degradation under humidity. Passivation is the key factor for sustaining the subthreshold properties and devices reliability. Based on our previous results, we will further study the effects of organic/inorganic passivation on a-IGZO TFTs. Passivation for a-IGZO TFT opens a potential way to fabricate high performance a-IGZO TFT with good reliability in ambience.

References

[1] H. Hosono, *J. Non-Cryst.Sol*, 352, 851-858 (2006)

[2] K. Nomura, H. Ohta, A. Takaji, T. Kamlya, M. Hirano, H. Hosono, *Nature* **432** 488 (2004)

[3] K. Nomura, A. Takagi, T. Kamiya, H. Ohta, M. Hirano, and H. Hosono, *Jpn. J. Appl. Phys.* **45**, 4303-4308 (2006).

[4] H. Yabuta, M. Sato, K. Abe, T. Aiba, T. Den, H. Kumomi, K. Nomura, T. Kamiya and H. Hosono, *Appl. Phys. Lett.*, **89**, 112123 (2006)

[5] C. J. Kim, D. H. Kang, I. H. Song, J. C. Park, H. Lim, S. I. Kim, E. H. Lee, R. J. Chung, J. C. Lee, and Y. S. Park, “High stable Ga_2O_3 - In_2O_3 - ZnO TFT for Active-Matrix Organic Light Emitting Diode Display Application”, *IEDM Tech. Dig.*, pp. **11.6.1-11.6.4**, 2005.

[6] J. Y. Kwon, K. S. Son, J. S. Jung, T. S. Kim, M. K. Ryu, K. B. Park, J. W. Kim, Y. G. Lee, C. J. Kim, S. I. Kim, Y. S. Park, S. Y. Lee, and J. M. K, *IDW, AMD* 9-3, (2007).

[7] P. Barquinha, A. M. Vila, G. Goncalves, L. Pereira, R. Martins, J. R. Morante, and E. Fortuato, *IEEE Transactions on Electron Devices*, Vol. **55**, No. 4, pp. **954-959**, (2008)

[8] J. Park, C. Kim, S. Kim, I. Song, S. Kim, D. Kang, H. Lim, H. Yin, R. Jung, E. Lee, J. Lee, K. Kwon, and Y. Park, *IEEE Electron Device Letters*, Vol. **29**, No. 8, pp. **879-881**, (2008).

[9] D. Kang, H. Lim, C. Kim, I. Song, J. Park, and Y. Park, *Appl. Phys.*

Lett. **90**, 123509 (2007).

- [11] K. Seshadri and C. D. Frisbie, *Appl. Phys Lett.* **78**, 993 (2001).
- [12] D. Natali, L. Fumagalli, and M. Sampietro, *J. Appl. Phys.* **101**, 12 (2007).
- [13] P. Barquinha, A. Villa, G. Gonclaves, L. Pereira, R. Martins, J. Morante, and E. Fortunato, *phys. Stat. sol (a)* **205**, No. 8, 1905-1909 (2008)
- [14] J. Park, J. Jeong. H. Chung, Y. Mo, and H. Kim, *Appl. Phys Lett.* **92**, 072104 (2008).
- [15] H. Hosono, *J. Non-Crystalline Solidst.* **352**, 351-358 (2006).
- [16] Y. T. Chou, et al “study on electrical properties of ZrZnO thin film transistor with dual stacks of gate dielectrics”, *ICMCTF* 2008.
- [17] J. Nishi, et al, *Jpn. J. Appl. Phys.* Vol. **42**, p. L347-L349 (2003).
- [18] P. F. Garcia, R. S. Mclean, and M. H. Reilly, *Appl. Phys. Lett.* **88**, 123509 (2006).
- [19] D. Kang, I. Song, C. Kim, Y. Park, *Appl. Phys. Lett.*, **91**, 091910 (2007)
- [20] H. Q. Chiang, B. R. Mcfarlane, D. Hong, R. E. Presley, J. F. Wager, *Journal of Non-Crystalline Solids*, **354**, 2826-2830 (2008)